NPS67-81-004

NAVAL POSTGRADUATE SCHOOL

Monterey, California

A STUDY OF NOTCH FATIGUE

PART I: STATIC PHOTOELASTIC MEASUREMENTS

GERALD H. LINDSEY

June 1981

Prepared for:
Naval Air Systems Command
Washington, DC 20361

NAVAL POSTGRADUATE SCHOOL

Monterey, California

Rear Admiral J. J. Ekelund
Superintendent

D. A. Schrady
Acting Provost

The work reported herein was supported by Naval Air Systems Command, Washington, DC.

This report was prepared by:

UNCLASSIFIED

SECURITY CLASSIFICATION OF THIS PAGE (When Data Entered)

REPORT DOCUMENTATION PAGE

READ INSTRUCTIONS BEFORE COMPLETING FORM

1. REPORT NUMBER: NPS67-81-004	2. GOVT ACCESSION NO.
3. RECIPIENT'S CATALOG NUMBER	
4. TITLE (and Subtitle): A STUDY OF NOTCH FATIGUE PART I: STATIC PHOTOELASTIC MEASUREMENTS	5. TYPE OF REPORT & PERIOD COVERED
	6. PERFORMING ORG. REPORT NUMBER
7. AUTHOR(s): Gerald H. Lindsey	8. CONTRACT OR GRANT NUMBER(s)
9. PERFORMING ORGANIZATION NAME AND ADDRESS: Naval Postgraduate School Monterey, California 93940	10. PROGRAM ELEMENT, PROJECT, TASK AREA & WORK UNIT NUMBERS: 61153N N0001981WR11104
11. CONTROLLING OFFICE NAME AND ADDRESS: Naval Air Systems Command Washington, DC 20361	12. REPORT DATE: June 1981 13. NUMBER OF PAGES: 80
14. MONITORING AGENCY NAME & ADDRESS (if different from Controlling Office)	15. SECURITY CLASS. (of this report): Unclassified 15a. DECLASSIFICATION DOWNGRADING SCHEDULE

16. DISTRIBUTION STATEMENT (of this Report)

Approved for public release; distribution unlimited.

17. DISTRIBUTION STATEMENT (of the abstract entered in Block 20, if different from Report)

18. SUPPLEMENTARY NOTES

19. KEY WORDS (Continue on reverse side if necessary and identify by block number)

Photoelasticity
Stress Concentration Factor
Oblique Incidence
Photoelastic Coating

20. ABSTRACT (Continue on reverse side if necessary and identify by block number)

A careful facility calibration of photoelastic measurements on uniaxial tension specimens containing stress concentrations was conducted. Thorough characterizations of both mechanical and optical properties were made in preparation for notch studies in the linear and nonlinear regimes. As a part of the work, a new elasticity solution is obtained to evaluate the effect on stress levels at the notch of Poisson's ratio mismatch between coating and specimen.

DD FORM 1 JAN 73 1473 EDITION OF 1 NOV 65 IS OBSOLETE
S/N 0102-014-6601

UNCLASSIFIED
SECURITY CLASSIFICATION OF THIS PAGE (When Data Entered)

TABLE OF CONTENTS

	PAGE
Introduction	1
Similitude	1
Geometric Similarity	3
Similitude in Uniaxial Tension	3
Photoelastic Material Properties	6
Selection	6
Characterization of PS-1C	8
Thickness Determination	8
Young's Modulus	9
Poisson's Ratio	12
Coating Fringe Value in Terms of Stress	12
Coating Fringe Value in Terms of Strain	12
Characterization of 7075-T6 Aluminum	14
Young's Modulus	16
Poisson's Ratio	21
Yield Stress & Strain Hardening Modulus	21
Ramberg-Osgood Coefficients	24
Reinforcement	26
Poisson's Ratio Mismatch	30
Experimental Comparison of Stress Concentration in a Strip Weakened by a Circular Hole	45
Experimental Procedure	45
Oblique Incidence	49
Calibrating the Polariscope	53
Generalizing for Any Material	56

Photoelastic Data for the Hole ---------- 57
Extrapolating to the Edge of the Hole ---------- 59
Accounting for Poisson's Ratio Mismatch ---------- 61
Check Against Numerical Solution ---------- 62
Check of Stress Distribution ---------- 63
Element Meshes ---------- 63
Using ADINA ---------- 65
Richardson Extrapolation ---------- 68
Optimal Stress Locations ---------- 70
Cicular Holes in Linear Material ---------- 70
Sensitivity Studies ---------- 74
Conclusions and Results ---------- 76
References ---------- 77
Appendix A ---------- 79

INTRODUCTION

Fatigue fractures occur at points of stress concentration, which are normally regions of complex stress distribution with large gradients. The stress field is geometry dependent and will only be reproduced in a laboratory sample if geometric similitude is preserved. Matching sample to part must also include similitude in the two major phases of fatigue; initiation and propagation and not merely a matching of stress concentration factors. In fact if the fatigue process were well understood, it would seem that a knowledge of the local conditions, coupled with material property information, would be all that is required to predict fatigue life.

This has not been possible so far, but this study has been undertaken to see how much success can be achieved toward this end via a detailed study of conditions surrounding the notch tip. To have any chance of success whatsoever, the local stress and strain conditions at the notch must be determined accurately. One of the means available for accomplishing this is experiment, and this approach was used successfully.

SIMILITUDE

An evaluation of how well one notch specimen models another can be studied via similitude theory. The strains in the vicinity of a notch depend upon the following variables:

$$\varepsilon_i = f_i(P, W, t, \rho, d, E, \nu) \qquad (1)$$

where ε_i = Strain components

P = Applied load

W = Sheet width

t = Sheet thickness

ρ = Radius of curvature of notch

d = Depth of notch

E = Tensile Modulus

ν = Poisson's Ratio

By dimensional analysis, the functional relationship can be written in terms of groupings of variables that are dimensionless.

$$\varepsilon_i = f_i\left(\frac{\sigma}{E}, \frac{W}{t}, \frac{d}{t}, \frac{\rho}{d}, \nu\right) \tag{2}$$

where

$$\sigma = \frac{P}{Wt}$$

From similitude theory, if in two different geometries

$$\frac{\sigma_1}{E_1} = \frac{\sigma_2}{E_2} \qquad \frac{d_1}{t_1} = \frac{d_2}{t_2} \qquad \frac{W_1}{t_1} = \frac{W_2}{t_2} \qquad \frac{\rho_1}{d_1} = \frac{\rho_2}{d_2}$$

$$\nu_1 = \nu_2$$

Then

$$\varepsilon_{i1} = \varepsilon_{i2}$$

GEOMETRIC SIMILARITY

If the material of the part and the model are the same, the same strains are produced only if they are geometrically similar. It is not sufficient to match only the stress at the notch tip, but complete similarity must be maintained. If the complete strain fields are not the same, the plastic zones will be different, and the neighborhood where fatigue action is taking place has different conditions. Thus, similarity must be preserved when employing experimental fatigue results from one specimen to predict fatigue failure in another. This is not generally done in current practice. Since it is not convenient, nor even practical, to run tests on a geometrically similar specimen each time a part is analyzed for fatigue, a different approach is attempted to develop a more general theory where knowledge of local conditions at the notch tip is sufficient, along with material properties, to predict fatigue in any specimen.

SIMILITUDE IN UNIAXIAL TENSION

Because much of the fatigue data available has been collected on uniaxial tension specimens and because something resembling uniaxial tension prevails at notch tips, it is reasonable to pursue this similarity, which is shown in Figure 1.

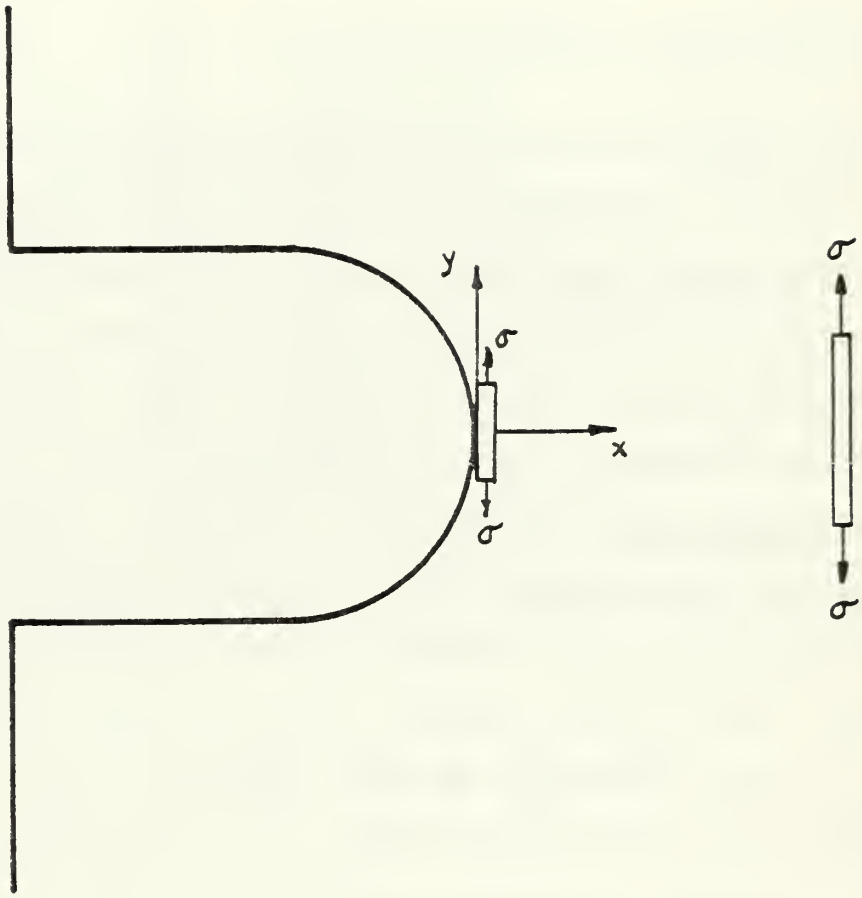

Figure 1. Uniaxial Model of Stress Condition at a Notch Tip.

For an elastic material

$$\varepsilon_i = f_i(\sigma_x, \sigma_y, \sigma_z, E, \nu) \tag{3}$$

If the same material is used for the model and the specimen, the strain field will be modeled to the degree that the stress field is modeled. For instance, in the region of

the notch tip in plane stress,

$$\varepsilon_x = \frac{1}{E}\left[\sigma_x - \nu\sigma_y\right] \tag{4}$$

To keep the departure from a uniaxial stress state less than 3%, which would be in the range of experimental measurement error, the transverse stress must be small.

$$\sigma_x \leq 0.03\,\nu\sigma_y \tag{5}$$

For a typical value of Poisson's Ratio for aluminum, $\nu = 0.33$ and

$$\sigma_x \leq 0.01\,\sigma_y \tag{6}$$

In the y direction,

$$\varepsilon_y = \frac{1}{E}\left[\sigma_y - \nu\sigma_x\right] \tag{7}$$

To maintain the same 3% limit,

$$\nu\sigma_x \leq 0.03\,\sigma_y$$

or

$$\sigma_x \leq 0.09\,\sigma_y \tag{8}$$

Also in the Z direction,

$$\sigma_x \leq 0.03\,\sigma_y \tag{9}$$

The most demanding of these is the first. In order to model the behavior at the notch tip as a uniaxial specimen, only regions may be considered where the radial stress is one per cent, or less, of the hoop stress.

For a circular hole in an infinite sheet, the location where $\sigma_r = 0.01\,\sigma_\theta$ is at $r = 1.0101\,a$. For a two inch diameter hole, the distance from the edge of the hole where the error exceeds the stated allowable is 0.01 in. This precludes the use of a strain gage to make local measurements. If specimen sizes were enlarged ten times until the uniaxial tensile region were large enough to accommodate a 1/8" strain gage, the hole would be twenty five inches in diameter and the specimen would be four to six feet wide and ten to twelve feet long. To circumvent this difficulty, photoelasticity was used as the experimental method for measuring local strain conditions at the notch. There are similar size problems, but they are not quite as severe as for strain gages, plus the bonus of obtaining the entire strain field at the notch tip made photoelasticity attractive.

PHOTOELASTIC MATERIAL PROPERTIES

SELECTION

7075-T6 aluminum was selected for the study of notch fatigue since it is a popular alloy of the aircraft industry and one for which there is a sizeable fatigue data base.

To coat 7075-T6 with a birefringent material that may be loaded into the plastic zone, Photolastic's PS-1 material was selected. It has a maximum strain capability of 10% and is a good all around photoelastic material.

Mil Handbook 5 gives typical data for 7075-T6 sheets of 0.080 in thickness. To extend into the yield range, strains of 10,000 μs must be measured with excursions up to 20,000 μs probably anticipated. From equation (A-1) of Appendix A, it is readily seen that

$$F_\varepsilon \sim \frac{\varepsilon}{N} \tag{10}$$

If something like five fringes are desired at the 10,000 μs level, the F_ε value needed is 0.002. This would allow 10 fringes at the maximum strain level expected.

From equation (A-4), the material fringe value is given by

$$f_\varepsilon = \frac{\lambda}{K} \tag{11}$$

For PS-1, the company supplied a value of K = 0.15, and for white light the wave length is $\lambda = 22.7 \times 10^{-6}$ in; thus the material fringe value is 1.5×10^{-4}. Using equation (A-1), the thickness of the coating desired is

$$h_c = \frac{f_\varepsilon}{2F_\varepsilon} = \frac{1.5 \times 10^{-4}}{(2)(.002)} = 0.038$$

The coating material PS-1C was purchased in sheets nominally .040 in thick. The bonding agent used was that suggested by Photolastic. At first PC-1 was used, but for higher elongations it was necessary to go to PC-8, even though the first cement was supposed to have the elongation capability required.

CHARACTERIZATION OF PS-1C PHOTOELASTIC MATERIAL

A careful characterization of PS-1C was conducted by Stenstrom (1) using two uniaxial tensile test specimens prepared from a single sheet of the photoelastic material. The first specimen was 1.0 inch wide and was used for thickness measurement and longitudinal strain data. The second 2.0 inch wide specimen was used for transverse strain data and for measuring the photoelastic coating stress fringe value, F_σ.

Thickness Determination

One longitudinal edge of the 1.0 inch wide specimen was lightly sanded to create a smooth, uniform cross-section of the photoelastic material. It was then mounted such that a traveling microscope could be used to measure thickness. With the contrast in appearance between the reflective coating and the base material, it was possible to accurately determine the thickness of each. For the specimen used, the base thickness was measured to be 0.0382 inches and the reflective

coating to be 0.0051 inches. These numbers were obtained by measuring eight separate points along the edge and averaging the results. The total average thickness of 0.0433 inches fell within the range of the manufacturer's measurement of 0.044±0.002 inches. It was therefore concluded that the labeled thickness included both the base and the reflective coating after two similar specimens of different marked thicknesses were checked. For calculation purposes, the thickness of the coating was taken to be 0.0382 inches since the path of polarized light does not penetrate the reflective coating of the photoelastic material. Inherent in using this thickness is the assumption that the reflective coating does not contribute to the reinforcement of the base material.

Young's Modulus

Two lines were lightly etched on the surface of the 1.0 inch wide specimen in the horizontal direction in order to accommodate a Tuckerman Optical Strain Gage. The specimen was then loaded in tension. The readings were taken with a autocollimater and recorded. Using the American Instrument Company calibration factors, the strain was calculated with the following formula taken from Ref. 2.

$$S = \frac{F \cdot A \cdot L \cdot R}{1000e} \qquad (12)$$

where S = Strain in microinches per inch

F = Lozenge calibration factor, = 1.002

A = Auto-collimater calibration factor, = 1.004

L = Lozenge length, 2.0 inches

R = Net reading

e = Gage length, 1.0 inch

With the measured strain, the measured load at each point and the known cross-sectional area, Young's Modulus, E, was determined from the slope of the stress-strain curve shown in Figure 1, using a linear regression analysis.

$$\sigma = 357,079.18\,\varepsilon_1 - 4.3407 \qquad (13)$$

$$R = 0.9988$$

where R = correlation coefficient.

Dropping the non-zero intercept, Young's modulus was taken to be

$$E_c = 357,079 \text{ psi} \qquad (14)$$

Photolastic Inc. information lists this modulus to be nominally 360,000 psi. Using thin specimens for this measurement requires very accurate thickness measurements because E is inversely proportional to thickness. Small errors in thickness can turn out to produce large percentage errors in area and modulus.

PS-1C CHARACTERIZATION
STRESS-STRAIN CURVE

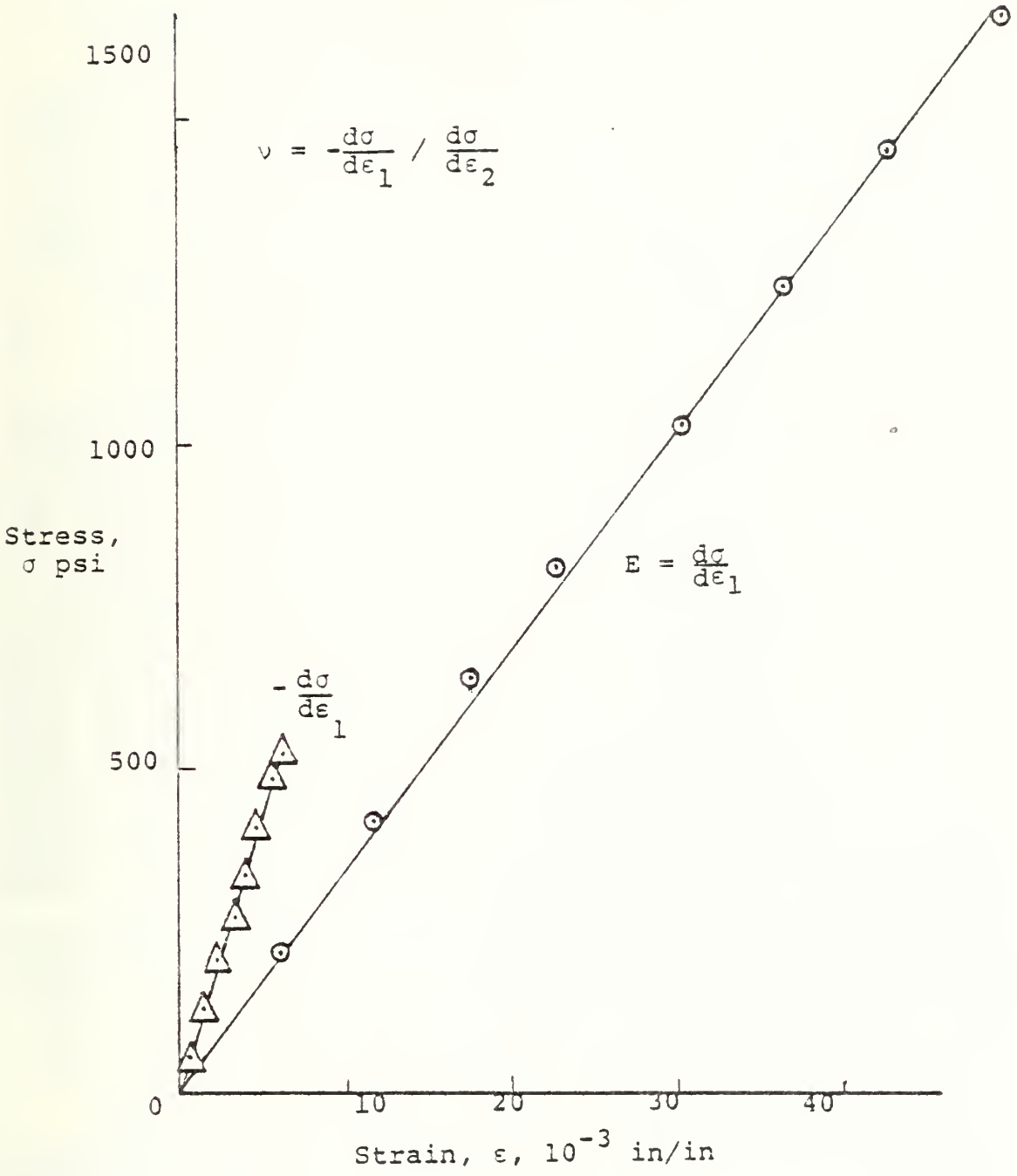

Figure 1

Poisson's Ratio

Using the 2.0 inch wide PS-1C specimen, two lines were lightly etched into the surface in the longitudinal direction one inch apart. With the Tuckerman Optical Strain Gage mounted in the transverse direction as shown in Figure 2, the specimen was loaded in tension. The data points from the test were used in a linear regression analysis with the following results:

$$\sigma = -941{,}487.02\,\varepsilon_L - 1.00708 \qquad (15)$$

$$R = 0.99991$$

Poisson's ratio was then determined by dropping the non-zero intercept and dividing the negative of the slope by E as indicated in Figure 1. The measured Poisson's ratio is

$$\nu_c = 0.3793$$

which compares with a nominal value of 0.38 supplied by Photolastic Inc. These tests were performed in accordance with ASTM standards for uniaxial properties (3).

Coating Fringe Value in Terms of Stress, F_σ

Prior to etching lines on the 2.0 inch wide specimen, it was loaded in tension in the elastic region, and the fringe number, N, was determined using a reflection polariscope. With several load points and known dimensions, the stress

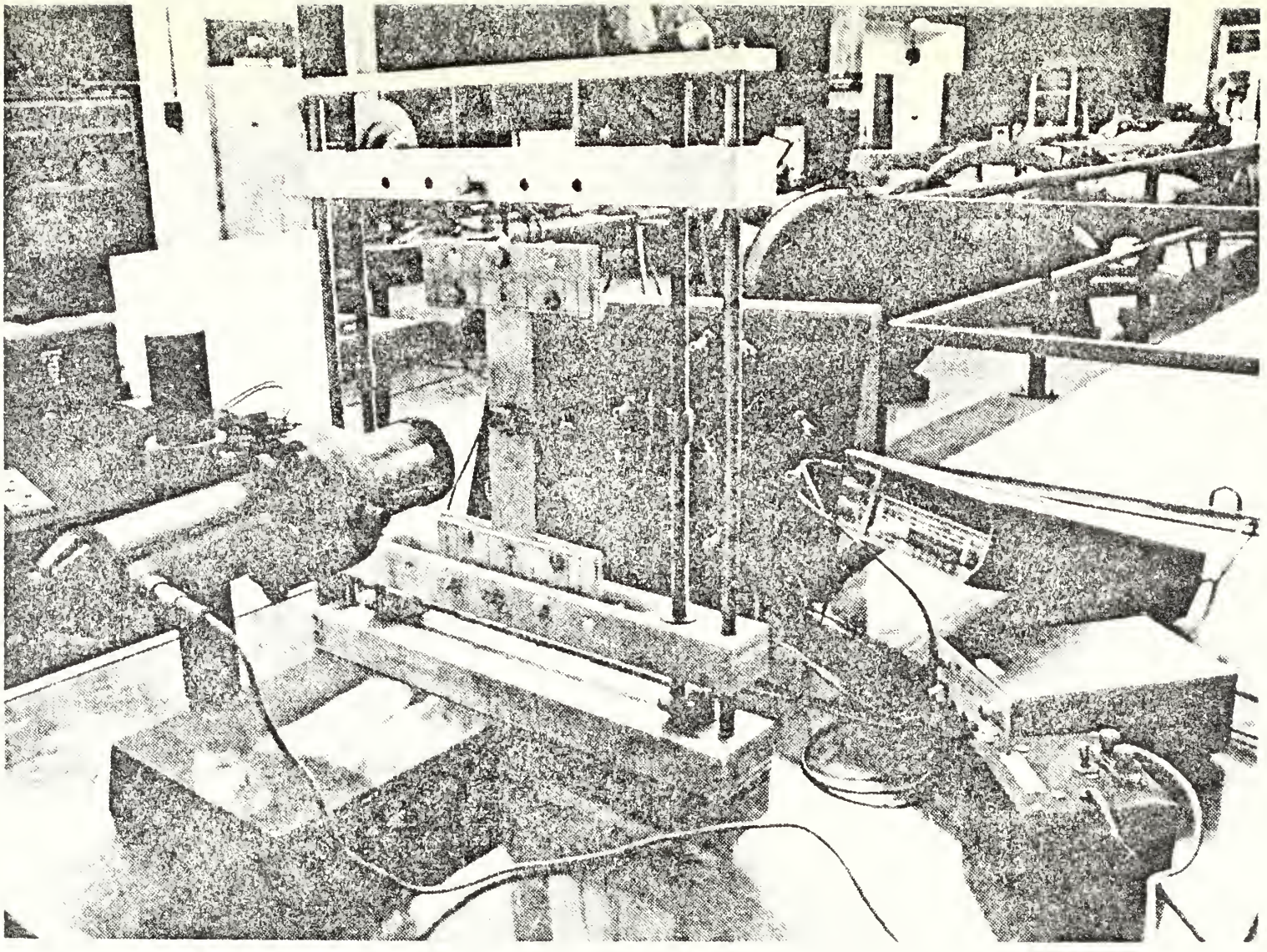

Figure 2. TUCKERMAN OPTICAL STRAIN GAGE SET-UP

was calculated and plotted against the fringe number. Using the data from Table I, a linear regression was made with the data which yielded

$$\sigma = 456.66 N + 1.9274 \tag{16}$$

$$R = .9993$$

Dropping the non-zero intercept, the stress fringe value was taken to be

$$F_\sigma = 456.67 \quad psi/fringe \tag{17}$$

Coating Fringe Value in Terms of Strain, F_ε

With the tensile modulus and the Poisson's Ratio of the coating material already determined, the strain coating fringe value can be calculated readily. From Appendix A,

$$F_\varepsilon = \frac{1+\nu_c}{E_c} F_\sigma = 1764 \times 10^{-6} \; in/in/fringe$$

CHARACTERIZATION OF 7075-T6

The elastic and plastic material properties of the aluminum panels were established by KAISER (4) using tensile tests of uniaxial specimens made from the same mill run as the sheets to be tested. The specimens were manufactured

TABLE I

PS-1C F_σ DETERMINATION

σ psi	Compensator Reading	N
0.0	0.0	0.0
202.37	23.0	0.489
408.42	39.0	0.830
610.26	63.0	1.340
785.26	79.5	1.691
990.53	102.0	2.170
1189.21	123.0	2.617

LINEAR REGRESSION:

$\sigma = 456.6661N + 1.92740$

$R = .99932$

and tested according to ASTM standards E8 and B557. (3) The specimens were cut transverse to the rolling direction, and the tests were performed in a 100 Kip MTS machine. The duration of the tests was three minutes. MICRO-MEASUREMENTS, EA-13-125AD-120, precision strain gages with a temperature compensated bridge circuit were used on all specimens. Transverse gage sensitivity errors were corrected according to the manufacturer's recommendations (5). Critical cross-section measurements were made with a micrometer.

YOUNG'S MODULUS (E)

Tests were conducted using the specimen shown in Fig. 3 on the MTS test machine with 10,000 lb INSTRON grips, which gripped the specimen evenly. The results of testing three specimens are shown in Tables II to IV where all strain values have been corrected for transverse sensitivity. Linear regression of the first eight points in the elastic range of all three specimens gave

$$\sigma = 381.86 + 1.0117 \times 10^{7} \varepsilon \qquad (18)$$

with a correlation coefficient of $R^2 = 0.9997$. Ignoring the non-zero intercept as specified by ASTM

$$E = 10.12 \times 10^{6} \text{ psi} \qquad (19)$$

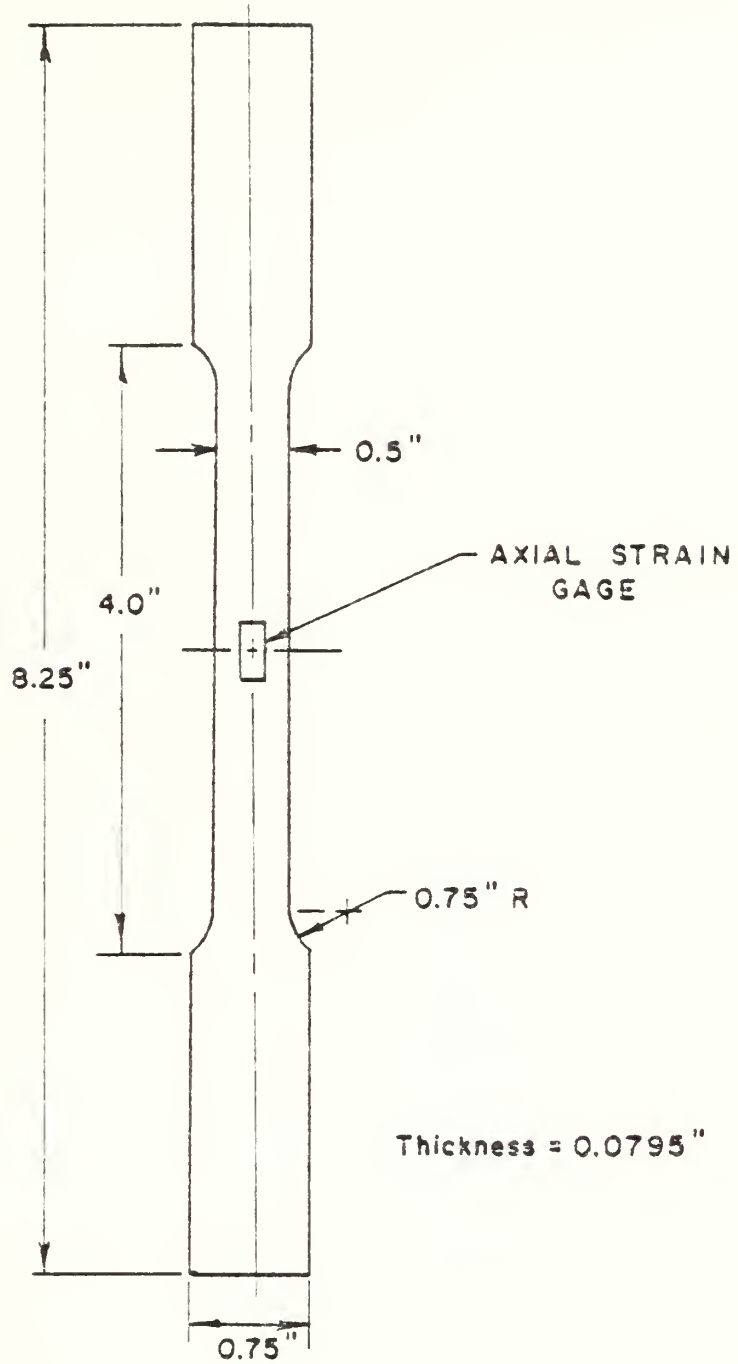

FIGURE 3 Characterization Specimen

TABLE II. MTS SPECIMEN A TEST RESULTS

Cross-section = 0.03975 in^2

Load, lbs.	Strain, $\varepsilon, 10^{-6}$ in/in
256	615
503	1204
750	1801
1005	2423
1255	3042
1505	3665
1778	4352
2003	4925
2252	5587
2508	6355
2755	7365
2905	8230
2984	9045
3037	10150

TABLE III. MTS SPECIMEN B TEST RESULTS

Cross-section = 0.03975 in^2

Load, lbs.	Strain, ϵ, 10^{-6} in/in
500	1250
750	1860
1000	2450
1250	3080
1500	3700
1750	4320
2000	4950
2250	5630
2500	6380
2750	7340
2900	8200
3000	9250
3050	10200
3100	11550
3125	12800

TABLE IV. MTS SPECIMEN C TEST RESULTS

Cross-section = 0.03975 in^2

Load, lbs.	Strain, ε, 10^{-6} in/in
272	663
503	1220
762	1850
1008	2451
1231	3005
1506	3690
1755	4318
2000	4940
2255	5607
2503	6325
2750	7230
2900	8120
3000	9200
3060	10500
3100	11500
3125	12500

POISSON'S RATIO (ν)

Tests were conducted using the specimen shown in Fig. 4 on the RIEHLE test machine with 10,000 lb RIEHLE grips. The results were tabulated in Table V. The transverse strain measurements were corrected by the manufacturer's data on transverse sensitivity. Both strains were read at the same load and plotted versus one another. A linear regression was made on the data resulting in:

$$\varepsilon_2 = 0.0000 - 0.3256\,\varepsilon_1 \qquad (20)$$

with a correlation coefficient of R = 0.99998. Disregarding the constant factor as insignificant to four places

$$\nu = 0.3256 \qquad (21)$$

YIELD STRESS AND STRAIN HARDENING MODULUS

The values of yield stress and strain hardening modulus were determined graphically using the data from Tables III and IV. Plastic region data in Table II is not reliable because of excessive creep encountered during that test.

0.2% offset yield stress, σ_y = 76,000 psi

strain hardening modulus, E_t = 566,000 psi

FIGURE 4

2 GAGE SPECIMEN

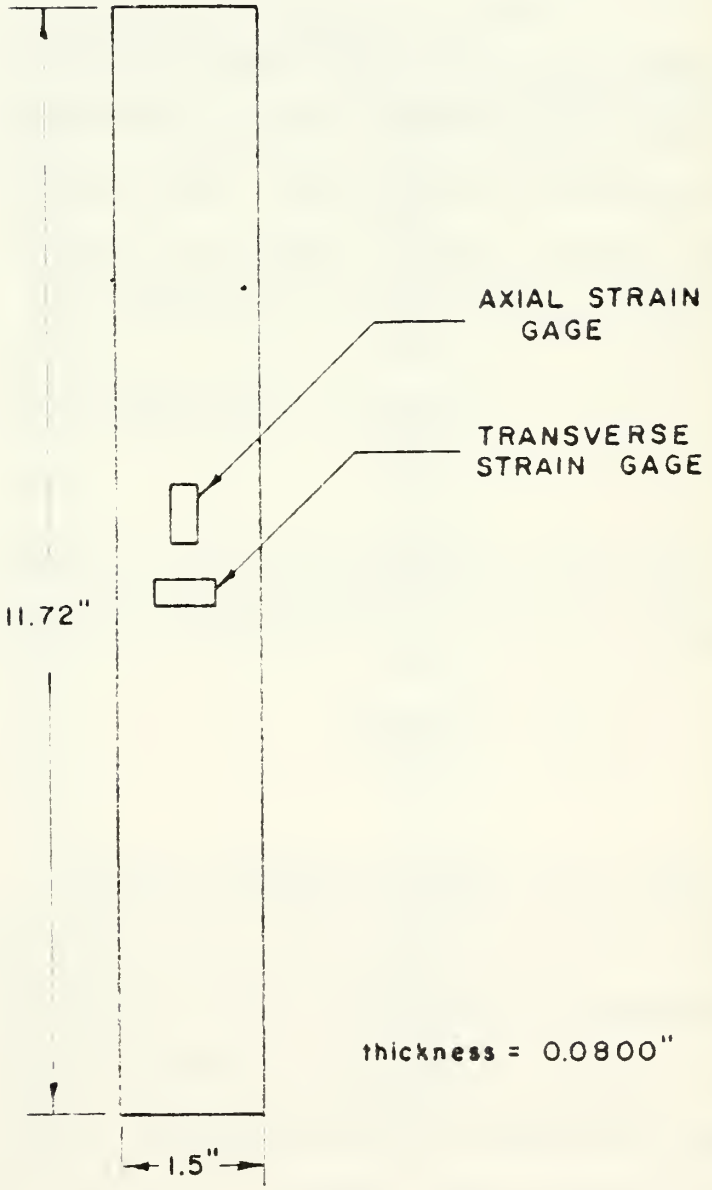

TABLE V. REIHLE SPECIMEN TEST RESULTS

Cross-section = 0.12 in^2

LOAD lbs.	STRAIN, ε_1 10^{-6} in/in	STRAIN, ε_2 10^{-6} in/in
500	345	-115
1000	720	-240
1500	1114	-364
2000	1501	-492
2500	1895	-614
3000	2291	-745
3500	2705	-871
4000	3095	-998
4500	3515	-1126
5000	3912	-1255
5500	4332	-1384
6000	4750	-1520
6500	5188	-1647
7000	5595	-1784
7500	6075	-1928
8000	6649	-2108
8500	7385	-2375
9000	8663	-2888
9500	12245	-4435

The graphical fit of these values to the test data can be seen in Fig. 5.

RAMBERG-OSGOOD COEFFICIENTS

The Ramberg-Osgood equation for elastic-plastic stress-strain characterization is given by:

$$\varepsilon = \frac{\sigma}{E} + \beta\left(\frac{\sigma}{E}\right)^n \tag{22}$$

where:

ε = strain

σ = stress

E = Young's modulus.

The β and n coefficients were determined graphically from the data of Table IV, by the method given by Ramberg and Osgood (6).

$$\beta = \frac{3}{7}\left[\frac{E}{\sigma_{.7E}}\right]^{n-1} \tag{23}$$

$$n = 1 + \frac{\log\left(17/7\right)}{\log\left(\frac{\sigma_{.7E}}{\sigma_{.85E}}\right)} \tag{24}$$

Lines corresponding to slopes of 0.7E and 0.85E were laid out on the X-Y recorder plots of load versus longitudinal strain. Load values where the rays intersected the load-

FIGURE 5

7075-T6 ALUMINUM STRESS-STRAIN CURVE

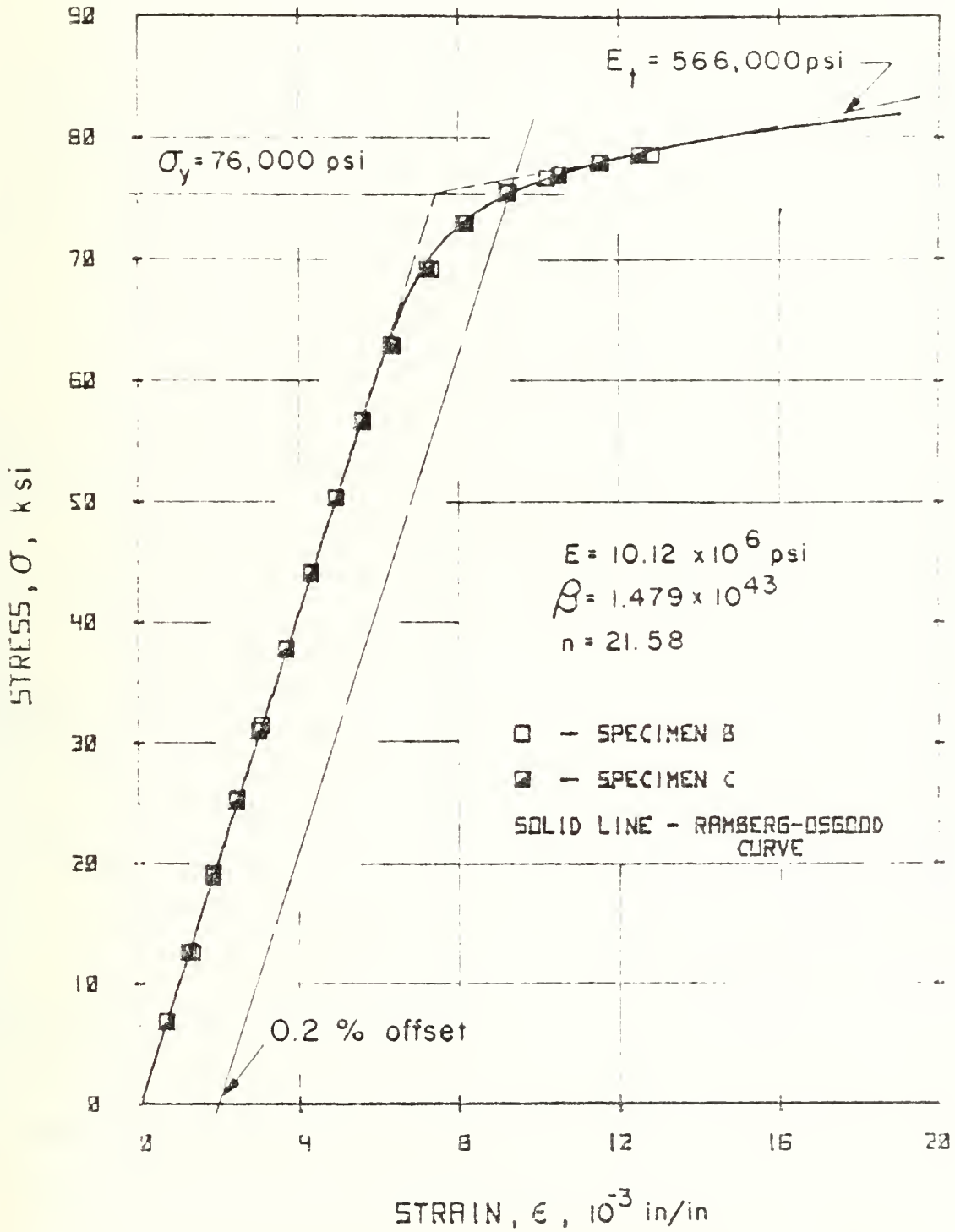

strain curve were

$$P_{.7E} = 3080 \text{ lbs} \qquad P_{.85E} = 2950 \text{ lbs}$$

The cross-sectional area from Fig. 3 is 0.03975 in^2. This gave

$$\sigma_{.7E} = 77{,}484 \text{ psi} \qquad \sigma_{.85E} = 74{,}214 \text{ psi}$$

The Ramberg-Osgood Parameters are given by

$$\beta = 1.479 \times 10^{43}$$

$$n = 21.58$$

The stress-strain law for uniaxial tension throughout the entire range is

$$\varepsilon = 9.881 \times 10^{-8} \sigma + .9949 \times 10^{-103} \sigma^{21.58} \qquad (25)$$

This is shown plotted in Fig. 5 along with data points from two of the specimens.

REINFORCEMENT

When specimens are made from thin sheets of material to duplicate wing skins, the coating material can provide some reinforcement to the specimen and influence the stress values. This is usually small, but since it is calculable

by classical developments, allowance can be readily made for it.

Consider an infinitesimal element in a biaxial stress field oriented along principal stress directions as illustrated in Fig. 6. If the total loads applied to the element are P_1 and P_2, they can be equated to the loads in the coating and the specimen,

$$P_1 = P_{1s} + P_{1c} \qquad P_2 = P_{2s} + P_{2c} \tag{26}$$

If there were no coating, the stress produced by P_1 and P_2 would be

$$P_1 = \sigma_{1u} h_s dx_2 \qquad P_2 = \sigma_{2u} h_s dx_1 \tag{27}$$

The stresses in the component parts of the coated specimen are given by

$$P_{1s} = \sigma_{1s} h_s dx_2 \qquad P_{2s} = \sigma_{2s} h_s dx_1 \tag{28}$$

$$P_{1c} = \sigma_{1c} h_c dx_2 \qquad P_{2c} = \sigma_{2c} h_c dx_1 \tag{29}$$

Equating the loads in the coated and the uncoated elements,

$$\sigma_{1u} h_s dx_2 = \sigma_{1s} h_s dx_2 + \sigma_{1c} h_c dx_2 \tag{30}$$

$$\sigma_{2u} h_s dx_1 = \sigma_{2s} h_s dx_1 + \sigma_{2c} h_c dx_1 \tag{31}$$

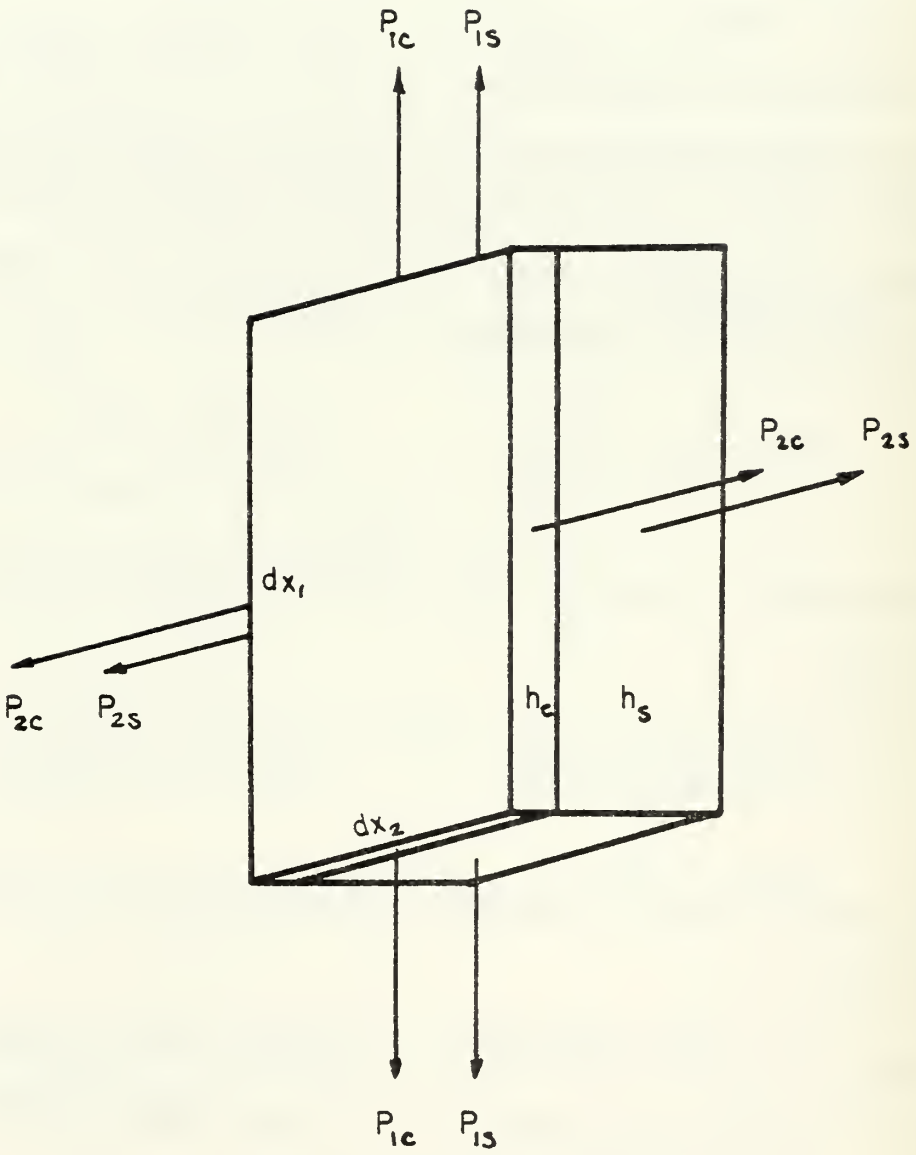

FIGURE 6. Reinforcement Model

Simplifying terms,

$$\sigma_{1u} = \sigma_{1s} + \frac{h_c}{h_s}\sigma_{1c} \tag{32}$$

$$\sigma_{2u} = \sigma_{2s} + \frac{h_c}{h_s}\sigma_{2c} \tag{33}$$

Subtracting the two equations

$$\sigma_{1u} - \sigma_{2u} = (\sigma_{1s} - \sigma_{2s}) + \frac{h_c}{h_s}(\sigma_{1c} - \sigma_{2c}) \tag{34}$$

From the plane stress constitutive equations,

$$\sigma_1 = \frac{E}{1-\nu^2}(\varepsilon_1 + \nu\varepsilon_2) \qquad \sigma_2 = \frac{E}{1-\nu^2}(\varepsilon_2 + \nu\varepsilon_1) \tag{35}$$

equation (34) can be transformed into expressions for strain

$$\frac{E_s}{1+\nu_s}(\varepsilon_{1u} - \varepsilon_{2u}) = \frac{E_s}{1+\nu_s}(\varepsilon_{1s} - \varepsilon_{2s}) + \frac{h_c}{h_s}\frac{E_c}{1+\nu_c}(\varepsilon_{1c} - \varepsilon_{2c}) \tag{36}$$

Recalling the fundamental characteristic of the photoelastic coating method.

$$\varepsilon_{1s} = \varepsilon_{1c} \qquad \varepsilon_{2s} = \varepsilon_{2c} \tag{37}$$

The reinforcement equation simplifies to

$$\varepsilon_{1u} - \varepsilon_{2u} = \left[1 + \frac{h_c}{h_s}\frac{E_c}{E_s}\frac{(1+\nu_s)}{(1+\nu_c)}\right](\varepsilon_{1c} - \varepsilon_{2c}) \tag{38}$$

The quantities in the bracket have all been measured; therefore all photoelastic measurements must be multiplied by this factor to obtain uncoated specimen response

$$\varepsilon_{1u} - \varepsilon_{2u} = 1.0162\ F_\varepsilon N \tag{39}$$

POISSON'S RATIO MISMATCH

As mentioned previously the notch tip may be considered, under certain restrictions, as a uniaxial specimen. As the tip is strained, the lateral contraction is different in the specimen and in the coating. At the interface of the coating and specimen,

$$\varepsilon_{2c} = \varepsilon_{2s} = -\nu_s \varepsilon_{1s} = -\nu_s \varepsilon_{1c} \tag{40}$$

at the free surface of the coating

$$\varepsilon_{2c} = -\nu_c \varepsilon_{1c} \tag{41}$$

Thus there is a transverse strain gradient through the thickness of the coating. The birefringence will exhibit the average strain readings, which will lie somewhere between the values at the interface and the values at the surface. At the interface,

$$\varepsilon_{1c} - \varepsilon_{2c} = \varepsilon_{1c}(1+\nu_s) = F_\varepsilon N \tag{42}$$

At the free surface,

$$\varepsilon_{1c} - \varepsilon_{2c} = \varepsilon_{1c}(1+\nu_c) = F_\varepsilon N \tag{43}$$

The actual fringe value, N, will be an average bounded by these two,

$$\frac{\varepsilon_{1c}}{F_\varepsilon}(1+\nu_s) < \bar{N} < \frac{\varepsilon_{1c}}{F_\varepsilon}(1+\nu_c) \tag{44}$$

Experiments with uniaxial tensile specimens have shown (7) that the strain variation through the thickness are only present near free boundaries in the plane of the specimen, such as the notch surface. This arises because of the edge effect.

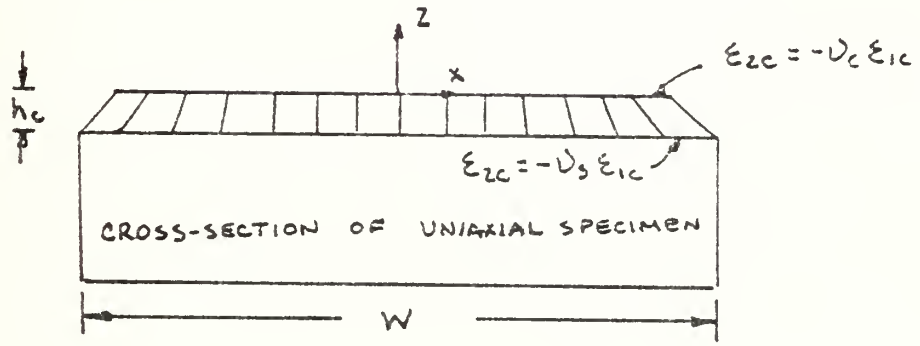

Describing the displacement field sketched above, we assume it to be of the following form:

$$u = u(x,z) \qquad v = v(y) \qquad w = w(z) \tag{45}$$

At $x = W/2$ there exists a contour for u which describes a curve in z

$$u\left(\frac{W}{2}, z\right) = g(z) \tag{46}$$

For instance $g(z) = (z^2 - h_c^2)$ yields a good solution; however for now we take a more general approach and only assume that $g(-h_c) = 0$.
This contour is continuously modified as one proceeds to the inner regions. This will be represented by

$$u(x,z) = f(x)\,g(z) \tag{47}$$

Since the displacement in the coating is not zero at the specimen boundary but rather produces a constant strain equal to that of the specimen, another term must be added.

$$u(x,z) = f(x)\,g(z) + C_1 x \tag{48}$$

The other displacements are chosen to give constant strains

$$v(y) = C_2 y \tag{49}$$

$$w(z) = C_3 z \tag{50}$$

The strains become

$$\varepsilon_x = \frac{\partial u}{\partial x} = f'(x)\, g(z) + C_1$$

$$\varepsilon_y = \frac{\partial v}{\partial y} = C_2$$

$$\varepsilon_z = \frac{\partial w}{\partial z} = C_3 \qquad (51)$$

$$\gamma_{xy} = \frac{\partial u}{\partial y} + \frac{\partial v}{\partial x} = 0$$

$$\gamma_{xz} = \frac{\partial u}{\partial z} + \frac{\partial w}{\partial x} = f(x)\, g'(z)$$

$$\gamma_{yz} = \frac{\partial v}{\partial z} + \frac{\partial w}{\partial y} = 0$$

The stresses become

$$\sigma_x = \frac{E_c}{1+\nu_c}\left[f'g + C_1\right] + \lambda_c\left[f'g + C_1 + C_2 + C_3\right]$$

$$\sigma_y = \frac{E_c}{1+\nu_c}\left[C_2\right] + \lambda_c\left[f'g + C_1 + C_2 + C_3\right] \qquad (52)$$

$$\sigma_z = \frac{E_c}{1+\nu_c}\left[C_3\right] + \lambda_c\left[f'g + C_1 + C_2 + C_3\right]$$

$$\tau_{xz} = G f g'$$

$$\tau_{yz} = 0$$

$$\tau_{xy} = 0$$

The general form of the stress expressions is:

$$\sigma_{ij} \sim F(x)G(z) + \text{Constant} \tag{53}$$

Using this general form as a guide, a more general solution is sought using the field equations. Assume $\tau_{xy} = \tau_{xz} = 0$ and $\frac{\partial}{\partial y} = 0$. The Equilibrium Equations simplify to

$$\frac{\partial \sigma_x}{\partial x} + \frac{\partial \tau_{xz}}{\partial z} = 0$$

$$\frac{\partial \tau_{xz}}{\partial x} + \frac{\partial \sigma_z}{\partial z} = 0 \tag{54}$$

These equations can be solved with a stress function by prescribing that

$$\sigma_x = \frac{\partial^2 \Phi}{\partial z^2} \qquad \tau_{xz} = -\frac{\partial^2 \Phi}{\partial x \partial z} \qquad \sigma_z = \frac{\partial^2 \Phi}{\partial z^2} \tag{55}$$

The Compatibility Equations reduce to

$$\nabla^2\sigma_x + \frac{1}{1+\nu_c}\frac{\partial^2\Theta}{\partial x^2} = 0 \qquad \Theta = \sigma_x + \sigma_y + \sigma_z$$

$$\nabla^2\sigma_y = 0$$

$$\nabla^2\sigma_z + \frac{1}{1+\nu_c}\frac{\partial^2\Theta}{\partial z^2} = 0 \tag{56}$$

$$\nabla^2\tau_{xz} + \frac{1}{1+\nu_c}\frac{\partial^2\Theta}{\partial x\partial z} = 0$$

Adding the first three compatibility equations gives

$$\left(\frac{2+\nu_c}{1+\nu_c}\right)\nabla^2\Theta = 0 \tag{57}$$

Since $\nabla^2\sigma_y = 0$

Then

$$\nabla^2(\sigma_x + \sigma_z) = 0 \tag{58}$$

Substituting the stress functions into (58), we obtain the governing equation for it.

$$\nabla^4\Phi = 0 \tag{59}$$

Using the biharmonic theorem,

$$\Phi = z\phi + \psi \tag{60}$$

where $\nabla^2\phi = 0$ and $\nabla^2\psi = 0$

Using separation of variables for ϕ and ψ

$$\phi = f(x)g(z) \qquad \psi = h(x)k(z) \tag{61}$$

the stress function can be represented as

$$\Phi(x,z) = z\,f(x)g(z) + h(x)k(z) \tag{62}$$

The stress of principal concern here is σ_x.

$$\sigma_x = f(x)\frac{d^2}{dz^2}\left[z\,g(z)\right] + h(x)\,k''(z) \tag{63}$$

To make it match the general form of equation (53), let

$$f(x) = 1 \qquad \frac{d^2}{dz^2}\left[z\,g(z)\right] = C_1 \tag{64}$$

g(z) is found by simple integration and h(x) and k(z) are found from solving LaPlace's Equation:

$$h(x) = A_1 \cosh \lambda x + A_2 \sinh \lambda x \tag{65}$$

$$k(z) = B_1 \cos \lambda z + B_2 \sin \lambda z \tag{66}$$

where λ is the separation parameter. The stress function is now determined.

$$\Phi = \frac{C_1 z^2}{2} + C_2 z + C_3 + (A_1 \cosh \lambda x + A_2 \sinh \lambda x)(B_1 \cos \lambda z + B_2 \sin \lambda z) \tag{67}$$

Differentiating, the stresses become

$$\sigma_x = C_1 - \lambda^2 (A_1 \cosh \lambda x + A_2 \sinh \lambda x)(B_1 \cos \lambda z + B_2 \sin \lambda z)$$

$$\sigma_z = \lambda^2 (A_1 \cosh \lambda x + A_2 \sinh \lambda x)(B_1 \cos \lambda z + B_2 \sin \lambda z) \tag{68}$$

$$\tau_{xz} = -\lambda^2 (A_1 \sinh \lambda x + A_2 \cosh \lambda x)(-B_1 \sin \lambda z + B_2 \cos \lambda z)$$

The normal stresses must be symmetric in x; therefore,

$$A_2 = 0$$

Without loss of generality, $A_1 = 1$. This simplifies the stress expressions somewhat to give,

$$\sigma_x = C_1 - \lambda^2 \cosh \lambda x (B_1 \cos \lambda z + B_2 \sin \lambda z)$$

$$\sigma_z = \lambda^2 \cosh \lambda x (B_1 \cos \lambda z + B_2 \sin \lambda z)$$

$$\tau_{xz} = \lambda^2 \sinh \lambda x (B_1 \sin \lambda z - B_2 \cos \lambda z) \tag{69}$$

We require that the shear stress be zero on the free surface $z = 0$. To accommodate this, B_2 is set equal to zero. The stresses simplify further to the form

$$\sigma_x = C_1 - \lambda^2 B_1 \cosh \lambda x \cos \lambda z$$

$$\sigma_z = \lambda^2 B_1 \cosh \lambda x \cos \lambda z \qquad (70)$$

$$\tau_{xz} = \lambda^2 B_1 \sinh \lambda x \sin \lambda z$$

Going back to the compatibility equations, others can now be satisfied. To start with,

$$\Theta = \sigma_x + \sigma_y + \sigma_z = C_1 + \sigma_y \qquad (71)$$

Because $\nabla^2 \sigma_x = 0$ from equation (70), equation (56) and (71) give

$$\frac{\partial^2 \Theta}{\partial x^2} = \frac{\partial^2}{\partial x^2}(C_1 + \sigma_y) = \frac{\partial^2 \sigma_y}{\partial x^2} = 0 \qquad (72)$$

Integrating,

$$\sigma_y = x F(z) + G(z) \qquad (73)$$

Substituting into equation (56)

$$x F''(z) + G''(z) = 0 \tag{74}$$

The only way that this can be satisfied for arbitrary values of x and z is for

$$F''(z) = 0 \qquad \text{and} \qquad G''(z) = 0 \tag{75}$$

Then upon integration,

$$F(z) = C_4 z + C_5 \qquad G(z) = C_6 z + C_7 \tag{76}$$

and

$$\sigma_y = x(C_4 z + C_5) + (C_6 z + C_7) \tag{77}$$

Since $\nabla^2 \sigma_z = 0$ from equation (70); then equation (56) gives

$$\frac{\partial^2 \Theta}{\partial z^2} = \frac{\partial^2}{\partial z^2}\left[C_1 + x(C_4 z + C_5) + (C_6 z + C_7)\right] = 0 \tag{78}$$

This is satisfied for all values of the constants. Since

$\nabla^2 \tau_{xz} = 0$ from equation (56)

$$\frac{\partial^2 \Theta}{\partial x \partial z} = \frac{\partial^2}{\partial x \partial z}\left[C_1 + x(C_4 z + C_5) + (C_6 z + C_7)\right] = 0 \tag{79}$$

This equation is satisfied if $C_4 = 0$; therefore, all of the field equations have been satisfied and

$$\sigma_y = C_5 x + C_6 z + C_7 \tag{80}$$

The strains in the plane of the coating are now of the form

$$\varepsilon_x = \frac{1}{E_c}\left[C_1 - B_1(1+\nu_c)\cosh\lambda x \cos\lambda z - \nu_c\left(C_5 x + C_6 z + C_7\right)\right]$$

$$\varepsilon_y = \frac{1}{E_c}\left[C_5 x + C_6 z + C_7 - \nu_c C_1\right] \tag{81}$$

The loading boundary conditions are: $\varepsilon_x = \varepsilon_{xs}$, $\varepsilon_y = \varepsilon_{ys}$ at $z = -h_c$. This gives

$$E_c\,\varepsilon_{xs} = \left[C_1 - B_1(1+\nu_c)\cosh\lambda x \cos\lambda h_c - \nu_c\left(C_5 x - C_6 h_c + C_7\right)\right]$$

$$E_c\,\varepsilon_{ys} = \left[C_5 x - C_6 h_c + C_7 - \nu_c C_1\right] \tag{82}$$

To satisfy these requirements, we set

$$\lambda = \frac{\pi}{2h_c} \quad \text{and} \quad C_5 = 0 \tag{83}$$

C_6 is set to zero to seek a solution for a constant σ_y. Since $\varepsilon_{xs} = -\nu_s \varepsilon_{ys}$, equations (82) simplify to

$$-\nu_s E_c \varepsilon_{ys} = C_1 - \nu_c C_7$$
$$E_c \varepsilon_{ys} = C_7 - \nu_c C_1 \tag{84}$$

Solving for the constants

$$C_1 = E_c \varepsilon_{ys} (\nu_c - \nu_s)$$
$$C_7 = E_c \varepsilon_{ys} \frac{(1 - \nu_c \nu_s)}{1 - \nu_c^2} \tag{85}$$

The last constant B_1 is found by setting the average transverse stress equal to zero at the boundary of the specimen. Assuming the specimen to be W units wide, $\bar{\sigma}_x = 0$ at $x = W/2$.

$$\bar{\sigma}_x \equiv \frac{1}{h_c} \int_{-h_c}^{0} \sigma_x \, dz \tag{86}$$

$$\bar{\sigma}_x = E_c \varepsilon_{ys} (\nu_c - \nu_s) - \frac{\pi}{2h_c^2} B_1 \cosh \frac{\pi W}{4h_c} = 0$$

From which,

$$B_1 = \frac{2h_c^2 E_c \varepsilon_{ys} (\nu_c - \nu_s)}{\pi \cosh\left(\frac{\pi W}{4h_c}\right)} \tag{87}$$

The stress expressions in final form are:

$$\sigma_x = E_c(\nu_c - \nu_s)\varepsilon_{ys}\left[1 - \frac{\pi}{2}\,\frac{\cosh\left(\frac{\pi x}{2h_c}\right)}{\cosh\left(\frac{\pi w}{4h_c}\right)}\cos\frac{\pi z}{2h_c}\right]$$

(88)

$$\sigma_y = \frac{E_c\left(1 - \nu_c\nu_s\right)}{\left(1 - \nu_c^2\right)}\varepsilon_{ys}$$

σ_z and τ_{xz} are neglected as being approximately zero compared to σ_y. As can be seen from the expression, if $\nu_c = \nu_s$, the stress state becomes uniaxial in the limiting condition; however, if there is a Poisson's Ratio mismatch, and there normally is, a transverse stress is created in the coating which influences to some degree the accuracy of the readings. This can be accounted for through this analysis by formulating an expression for an equivalent Poisson's Ratio. To do this we first formulate expressions for the average strains through the thickness of the coating, which will be what the fringes will be measuring.

$$\bar{\varepsilon}_x = \varepsilon_{ys}\left\{(\nu_c - \nu_s)\left[1 - \frac{\cosh\left(\frac{\pi x}{2h_c}\right)}{\cosh\left(\frac{\pi w}{4h_c}\right)}\right] - \frac{\nu_c(1 - \nu_c\nu_s)}{(1 - \nu_c^2)}\right\}$$

(89)

$$\bar{\varepsilon}_y = \varepsilon_{ys}\left\{\frac{(1 - \nu_c\nu_s)}{(1 - \nu_c^2)} - \nu_c(\nu_c - \nu_s)\left[1 - \frac{\cosh\left(\frac{\pi x}{2h_c}\right)}{\cosh\left(\frac{\pi w}{4h_c}\right)}\right]\right\}$$

An equivalent Poisson's Ratio is defined in the obvious way.

$$\bar{\nu} = -\frac{\bar{\varepsilon}_x}{\bar{\varepsilon}_y} \tag{90}$$

Substituting elastic material properties referred to earlier

$$\bar{\nu} = \frac{.3346 + .0537 \dfrac{\cosh\left(\frac{\pi x}{2h_c}\right)}{\cosh\left(\frac{\pi W}{4h_c}\right)}}{1.0034 + .0204 \dfrac{\cosh\left(\frac{\pi x}{2h_c}\right)}{\cosh\left(\frac{\pi W}{4h_c}\right)}} \tag{91}$$

A plot of this expression was made assuming that $W >> h_c$; for instance, let $W = 20h_c$. A plot of the behavior is shown in Fig. 7.

If the specimen material is taken into the plastic range where $\nu_s = 0.500$, the expression for Poisson's Ratio becomes

$$\bar{\nu} = \frac{.4797 - .1207 \dfrac{\cosh\left(\frac{\pi x}{2h_c}\right)}{\cosh\left(\frac{\pi W}{4h_c}\right)}}{.9923 - .0458 \dfrac{\cosh\left(\frac{\pi x}{2h_c}\right)}{\cosh\left(\frac{\pi W}{4h_c}\right)}} \tag{92}$$

For the same parameters of $W = 20h_c$, the plot of equivalent

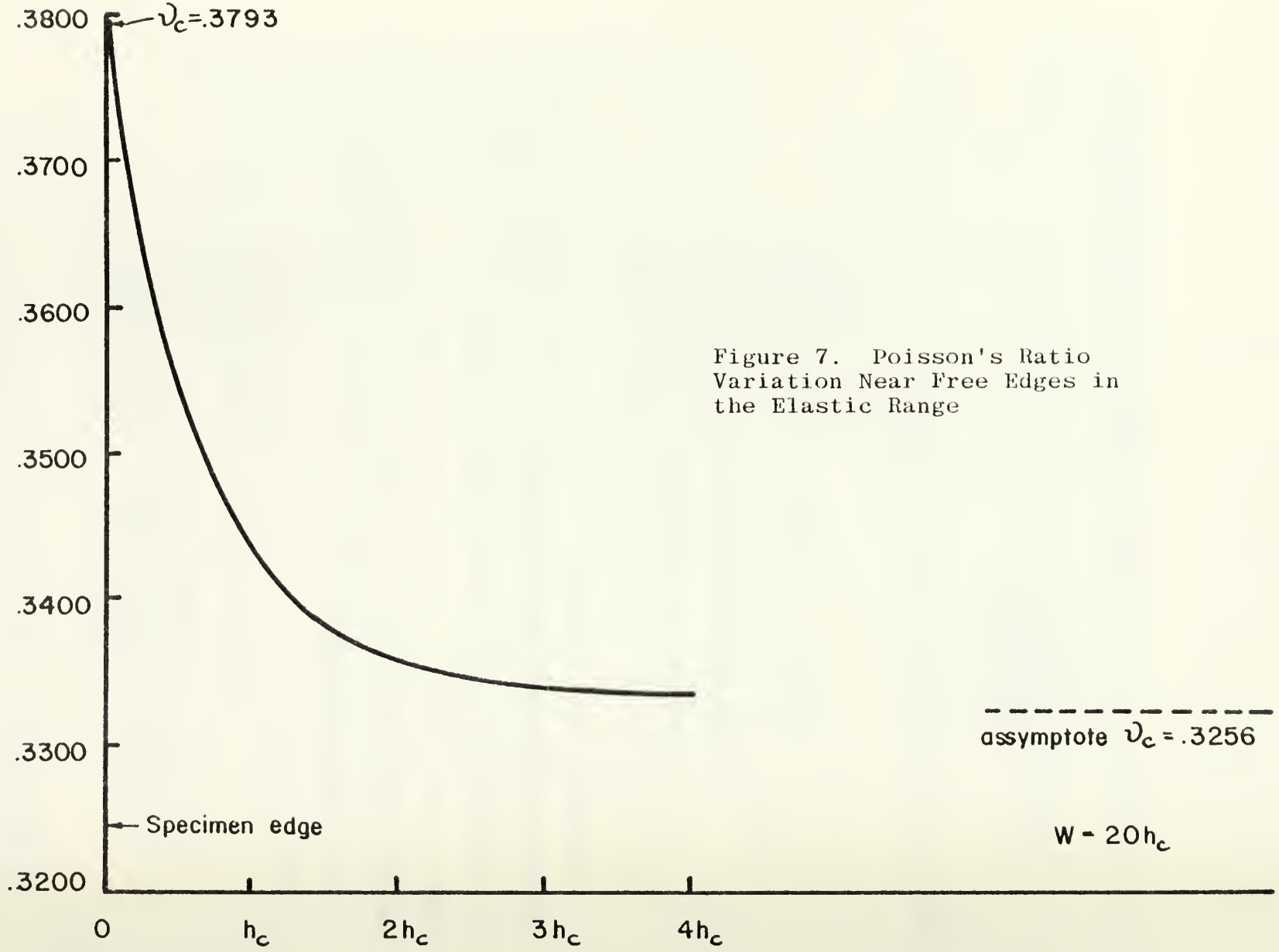

Figure 7. Poisson's Ratio Variation Near Free Edges in the Elastic Range

Poisson's Ratio for the plastic case is given in Fig. 8. In both cases the combined specimen has at the free boundary the Poisson's Ratio of the coating; however, this falls off rapidly as one moves to the interior. Within three or four coating thicknesses of the edge the Poisson's Ratio has approached a constant value, but it is different than the specimen value alone.

EXPERIMENTAL COMPARISON OF STRESS CONCENTRATION IN A STRIP WEAKENED BY A CIRCULAR HOLE

To test the validity and accuracy of utilizing the photoelastic method, a test case using a circular hole specimen of finite width was selected. R. C. J. Howland (8) determined the stress distribution around the circular hole and with the known theoretical solution, it was possible to determine the accuracy of the photoelastic method.

EXPERIMENTAL PROCEDURE

A specimen was designed to accommodate a 2.0 inch diameter hole in the center. To determine a reasonable width and length which would allow a uniaxial field to exist between the center hole and the end grips, a 1/8 scale PS-1C model was tested under various tensile load conditions. It was determined that a minimum of a five-to-one ratio for length-to-width must exist to eliminate interference of fringe patterns. Fig. 9 shows the geometry selected.

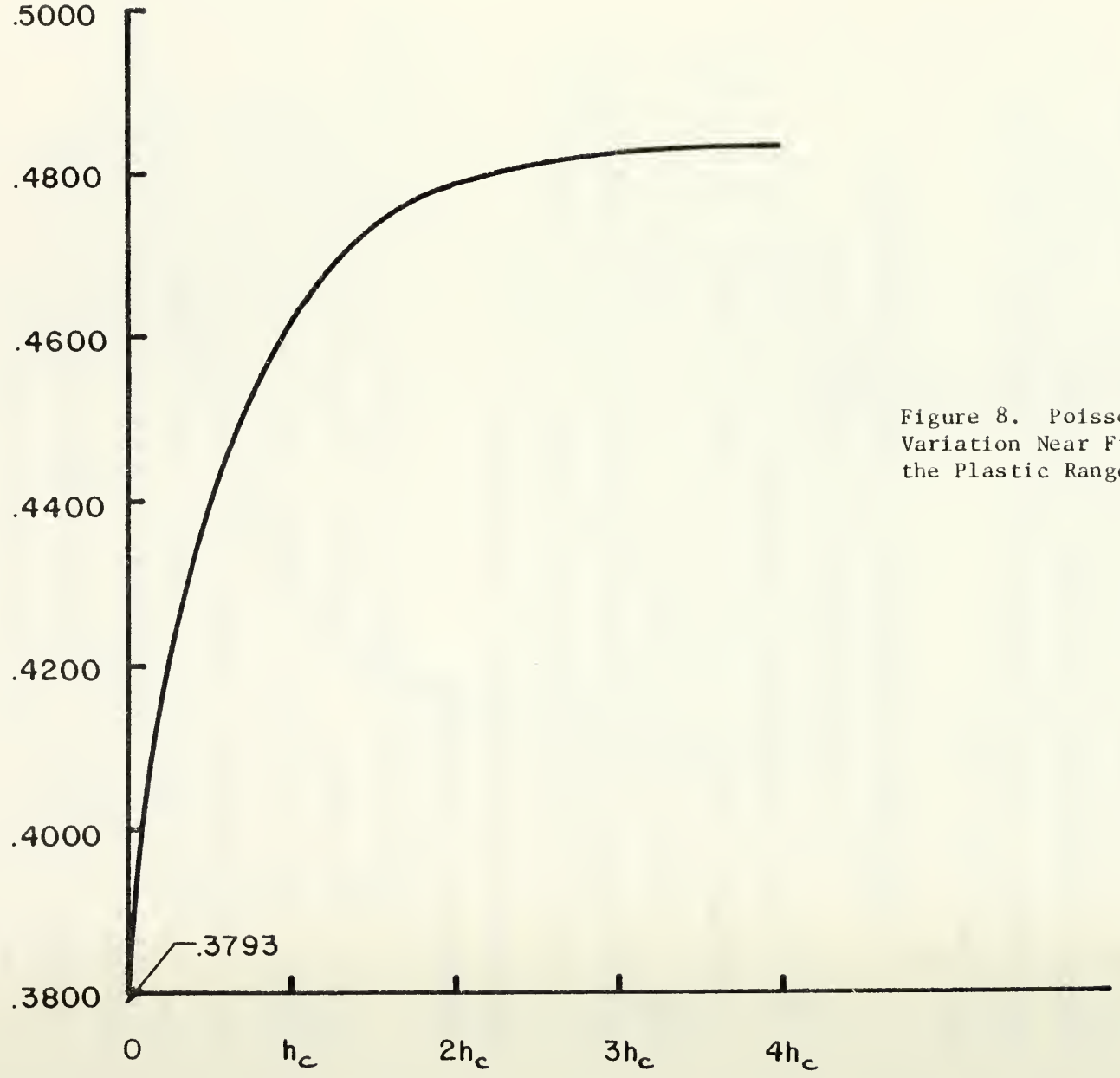

Figure 8. Poisson's Ratio Variation Near Free Edges in the Plastic Range

CIRCULAR HOLE SPECIMEN

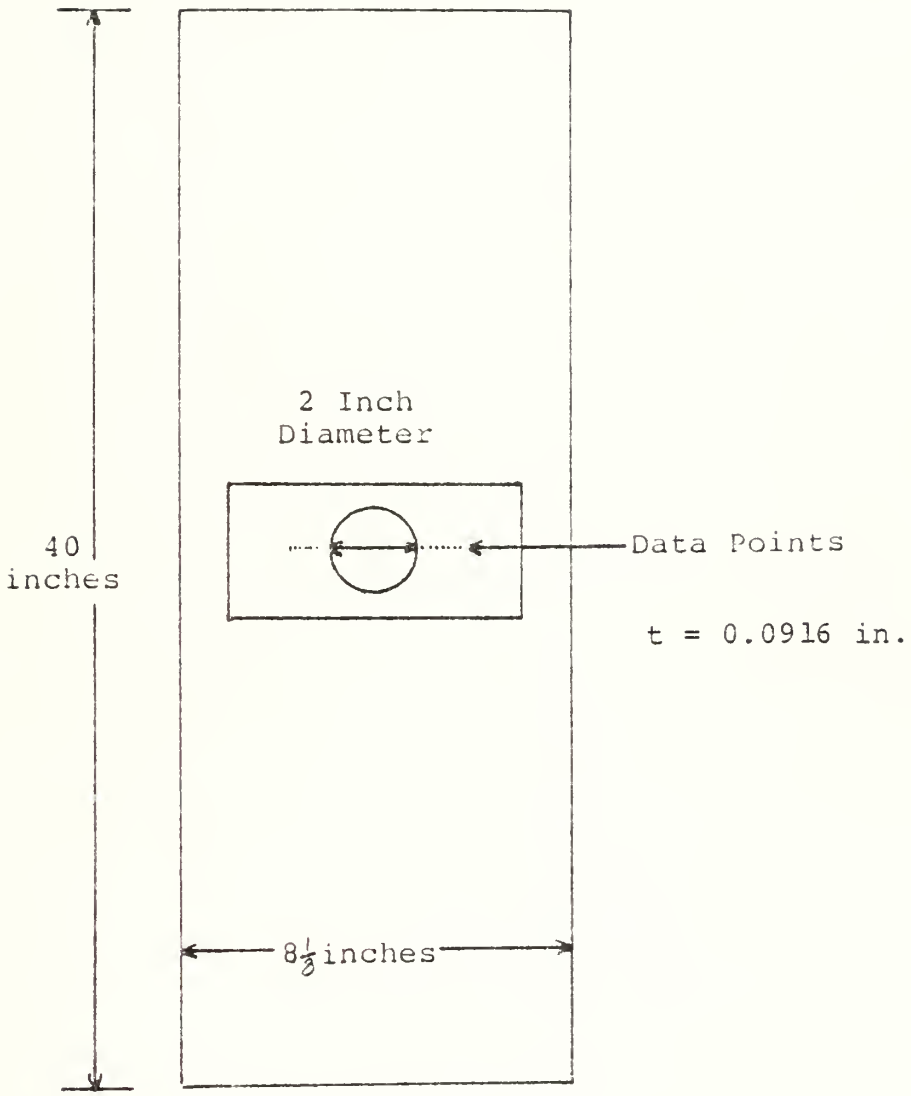

Figure 9

The aluminum specimen was placed under an 8000 pound load in the MTS machine, and compensator readings were taken with a Model 032 Photolastic Compensator at the 90° position on each side of the hole. They were found to be 122 / 121 counts, or an average of 121.5 counts. The strain-optic equation from Appendix A can be written as

$$\varepsilon_y - \varepsilon_x = F_\sigma \frac{(1+\nu_c) N}{E_c} \tag{93}$$

At the circular boundary, $\varepsilon_x = -\nu_c \varepsilon_y$

$$\varepsilon_y = \frac{F_\sigma N}{E_c} = 0.003295 \text{ in/in} \tag{94}$$

Making the correction for reinforcement,

$$\varepsilon_y^u = 1.0163\, \varepsilon_y = 0.003348 \text{ in/in} \tag{95}$$

The local hoop stress is

$$\sigma_y^u = E_s \varepsilon_y^u = 33,886 \text{ psi} \tag{96}$$

Howland's results for this case gave 34,719 psi at the edge of the hole. This indicates a difference of 2.4%. Later we will show that this difference is reduced by more than a factor of three by extropolating to determine the surface

stress from readings in the interior.

OBLIQUE INCIDENCE

In order to determine stress values away from the edge of the hole, oblique incidence was used. Fig. 10 is a schematic showing the coordinate system for rotation about the Y axis. The governing equations become,

$$N = \frac{2h_c}{f_\varepsilon}(\varepsilon_y - \varepsilon_x) \tag{97}$$

$$N_{\theta y} = \frac{2h_c}{f_\varepsilon}(\varepsilon_y - \varepsilon_x') \tag{98}$$

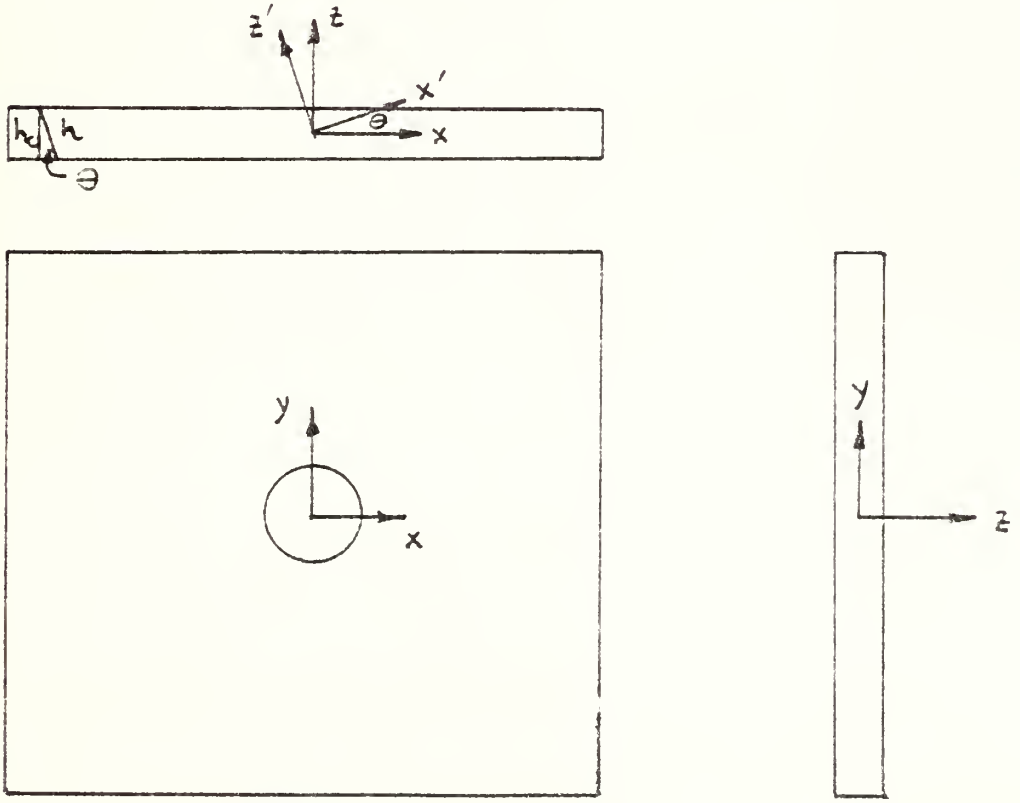

Figure 10. Oblique Incidence Coordinates for Rotation about the y axis.

The strain in the x' direction is given from the strain transformation laws

$$\varepsilon_x' = \varepsilon_x \cos^2\theta + \varepsilon_z \sin^2\theta \tag{99}$$

For plane stress, the following stress-strain relationships hold:

$$\varepsilon_z = -\frac{\nu_c}{E_c}\left(\sigma_{xc} + \sigma_{yc}\right) \tag{100}$$

$$\sigma_{xc} = \frac{E_c}{1-\nu_c^2}\left[\varepsilon_x + \nu_c \varepsilon_y\right] \tag{101}$$

$$\sigma_{yc} = \frac{E_c}{1-\nu_c^2}\left[\varepsilon_y + \nu_c \varepsilon_x\right] \tag{102}$$

Putting these together,

$$\varepsilon_z = -\frac{\nu_c}{1-\nu_c}\left(\varepsilon_x + \varepsilon_y\right) \tag{103}$$

and the expression of strain along the oblique axis becomes

$$\varepsilon_x' = \varepsilon_x \cos^2\theta - \frac{\nu_c}{1-\nu_c}\left(\varepsilon_x + \varepsilon_y\right)\sin^2\theta \tag{104}$$

From Fig. 10 it can be seen that $h_c = h\cos\theta$. Putting all of these expressions into Equation (98), an equation for $N_{\theta y}$ in terms of known quantities can be obtained.

$$N_{\theta y} = \frac{2h_c}{f_\varepsilon}\left[\frac{1}{(1-\nu_c)\cos\theta}\right]\left[\varepsilon_y(1-\nu_c\cos^2\theta)+\varepsilon_x(\nu_c-\cos^2\theta)\right] \quad (105)$$

Solving this equation simultaneously with equation (97),

$$\varepsilon_x = \frac{F\varepsilon}{(1+\nu_c)\sin^2\theta}\left[N_{\theta y}(1-\nu_c)\cos\theta - N(1-\nu_c\cos^2\theta)\right] \quad (106)$$

$$\varepsilon_y = \frac{F\varepsilon}{(1+\nu_c)\sin^2\theta}\left[N_{\theta y}(1-\nu_c)\cos\theta - N(\cos^2\theta-\nu_c)\right] \quad (107)$$

For rotation about the other axis,

$$N_{\theta x} = \frac{2h}{f_\varepsilon}\left(\varepsilon_y' - \varepsilon_x\right) \quad (108)$$

Fig. 11 shows a schematic of this oblique incidence arrangement. The strain in the oblique direction turns out to be of the same form as before.

$$\varepsilon_y' = \varepsilon_y\cos^2\theta + \varepsilon_z\sin^2\theta \quad (109)$$

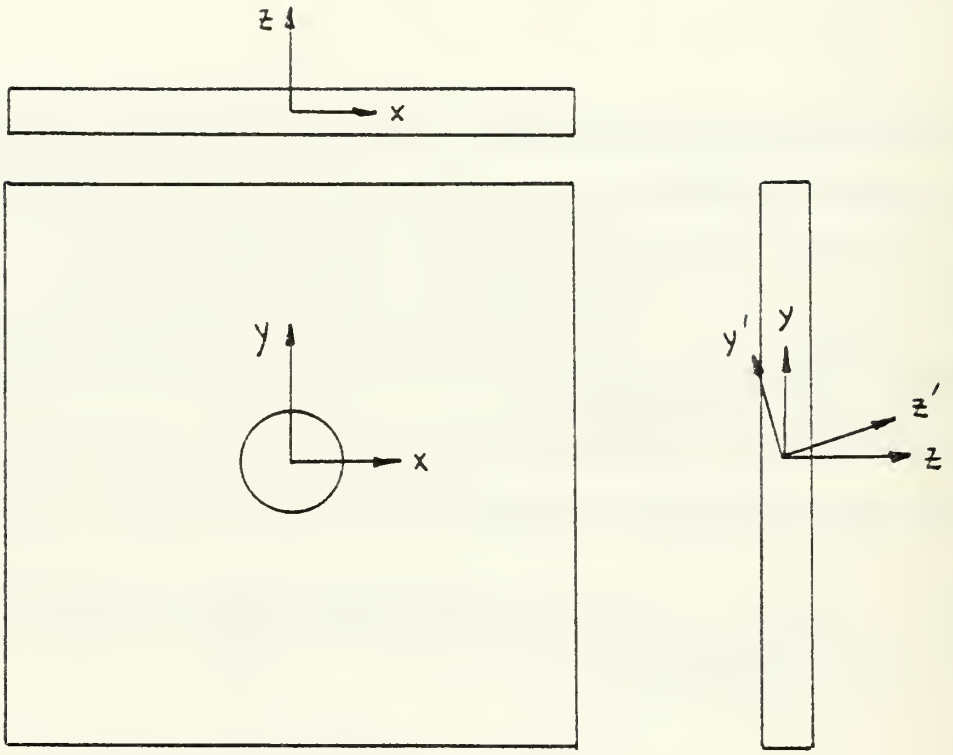

Figure 11. Oblique Incidence Coordinates for Rotation about the x axis.

Using the expresion for ε_z previously derived and the expression for h, the expression for the oblique fringe value becomes

$$N_{\theta x} = \frac{2h_c}{f_\varepsilon}\left[\frac{1}{(1-\nu_c)\cos\theta}\right]\left[\varepsilon_y\left(\cos^2\theta - \nu_c\right) - \varepsilon_x\left(1 - \nu_c\cos^2\theta\right)\right] \quad (110)$$

Solving this simultaneously with the normal incidence equation (97), the strain expressions are:

$$\varepsilon_x = \frac{F\varepsilon}{(1+\nu_c)\sin^2\theta}\left[N\left(\cos^2\theta - \nu_c\right) - N_{\theta x}\left(1-\nu_c\right)\cos\theta\right] \quad (111)$$

$$\varepsilon_y = \frac{F_\varepsilon}{(1+\nu_c)\sin^2\theta}\left[N(1-\nu_c\cos^2\theta) - N_{\theta x}(1-\nu_c)\cos\theta\right] \quad (112)$$

Calibrating the Polariscope

In oblique incidence the determination of the angle can be tedious because of changes in it at the surface due to the index of refraction being different in the coating than it is in air. The light ray is bent as shown in Fig. 12. It is more reliable to obtain the value experimentally. For instance, equations (106), (107) (111) and (112) can be written as

$$\varepsilon_x = F_\varepsilon\left[A N_{\theta y} - C N\right] \quad (113)$$

$$\varepsilon_y = F_\varepsilon\left[A N_{\theta y} - B N\right] \quad (114)$$

$$\varepsilon_x = F_\varepsilon\left[B N - A N_{\theta x}\right] \quad (115)$$

$$\varepsilon_y = F_\varepsilon\left[C N - A N_{\theta x}\right] \quad (116)$$

Subtracting (114) from (113) or (115) from (116),

$$\varepsilon_y - \varepsilon_x = N F_\varepsilon (C-B) \quad (117)$$

Since C - B = 1 from the basic equation (A-1),

$$C = B + 1$$

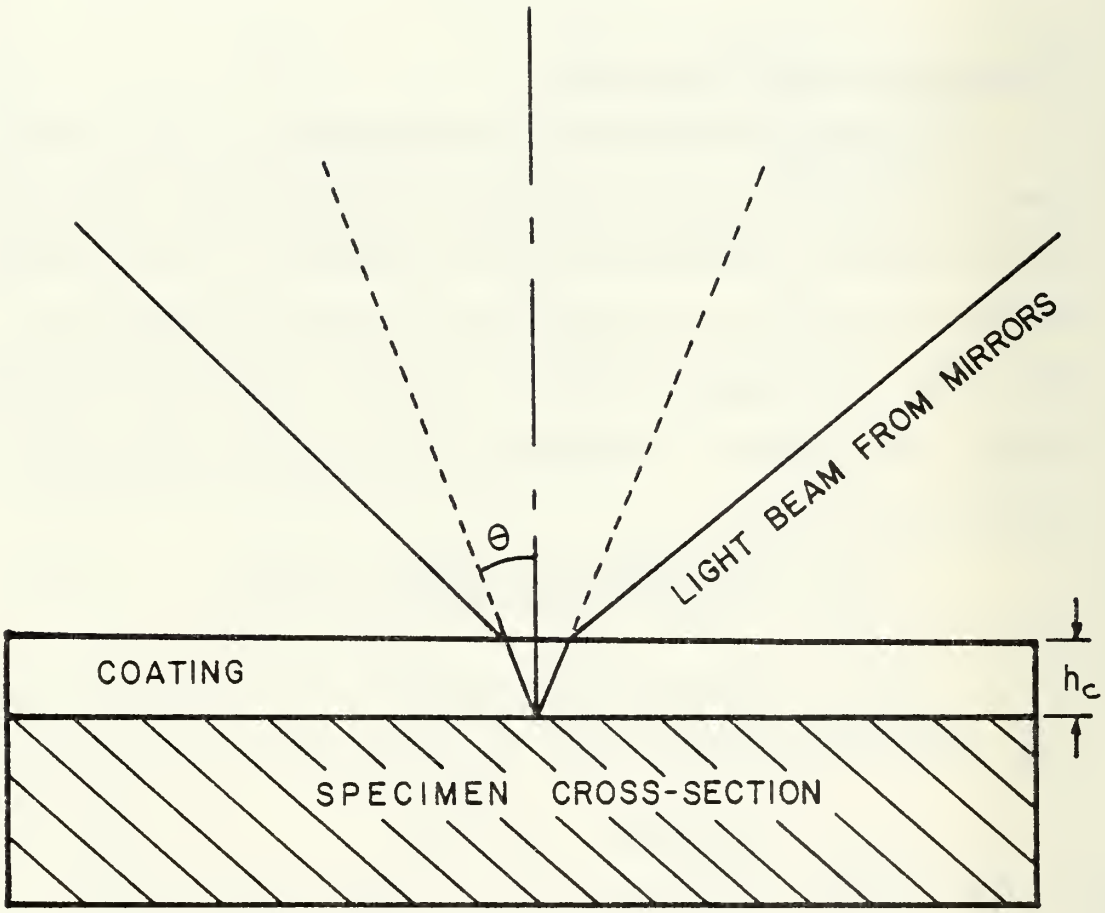

Figure 12. Definition of Angle of Refraction for the Polariscope

Solving two of the other equations simultaneously for A and B,

$$A = \frac{(\varepsilon_y + \varepsilon_x) N}{(\varepsilon_y - \varepsilon_x)(N_{\theta y} - N_{\theta x})} \tag{118}$$

$$B = \frac{\varepsilon_y N_{\theta x} + \varepsilon_x N_{\theta y}}{(\varepsilon_y - \varepsilon_x)(N_{\theta y} - N_{\theta x})} \tag{119}$$

Using a uniaxial test to make the calibration tests, the expression for A, B and C become

$$A = \frac{(1-\bar{\nu}) N}{(1+\bar{\nu})(N_{\theta y} - N_{\theta x})} \tag{120}$$

$$B = \frac{N_{\theta x} - \bar{\nu} N_{\theta y}}{(1+\bar{\nu})(N_{\theta y} - N_{\theta x})} \tag{121}$$

$$C = B + 1 \tag{122}$$

Several readings were made of normal incidence and both oblique incidence fringes on a uniaxial specimen of coating material at different load levels. $N_{\theta x}$ and $N_{\theta y}$ were plotted versus N and a linear regression was made of the data.

$$N_{\theta x} = 0.510 + 0.856 N \tag{123}$$

$$R = 0.9989$$

$$N_{\theta y} = -2.188 + 1.184\, N \qquad (124)$$

$$R = 0.9997$$

Substituting into equations (120) to (122) and using $\bar{\nu} = \nu_c = 0.3793$, the constants were found to be

A = 1.372

B = 0.899

C = 1.899

Generalizing for Any Material

In order to use the equations of oblique incidence for measurements on materials of any Poisson's Ratio, the expressions for the constants were used to solve for the overall incidence angle θ.

$$A = \frac{(1-\nu_c)\cos\theta}{(1+\nu_c)\sin^2\theta} = 1.372 \qquad (125)$$

Solving this equation, $\theta = 31.85^\circ$. The other two expressions for B and C both gave $\theta = 31.76^\circ$. The good agreement gave confidence in the numbers, and the average value of 31.8° will be used in all further calculations.

The expressions for strain in terms of N and $N_{\theta y}$ become

$$\varepsilon_x = \frac{F\varepsilon}{1+\bar{\nu}}\left[3.0607(1-\bar{\nu})N_{\theta y} - (3.6012 - 2.6012\bar{\nu})N\right] \quad (126)$$

$$\varepsilon_y = \frac{F\varepsilon}{1+\bar{\nu}}\left[3.0607(1-\bar{\nu})N_{\theta y} - (2.6012 - 3.6012\bar{\nu})N\right] \quad (127)$$

For rotations about the x axis,

$$\varepsilon_x = \frac{F\varepsilon}{1+\bar{\nu}}\left[(2.6012 - 3.6012\bar{\nu})N - 3.0607(1-\bar{\nu})N_{\theta x}\right] \quad (128)$$

$$\varepsilon_y = \frac{F\varepsilon}{1+\bar{\nu}}\left[(3.6012 - 2.6012\bar{\nu})N - 3.0607(1-\bar{\nu})N_{\theta x}\right] \quad (129)$$

PHOTOELASTIC DATA FOR THE HOLE

Normal and oblique compensator readings were taken at 0.0625 inch intervals at the 90° position on each side of the hole as shown in Fig. 9 for a loading of 12,000 lbs., or a far-field stress of 16,124 psi. Six different compensator readings were made by two observers; i.e. each observer made three readings, and these are listed in Table VI. The average and standard deviation are also listed.

TABLE VI

CIRCULAR HOLE COMPENSATOR READINGS

NORMAL INCIDENCE

X							AVG.	STD DEV
0.0625	148	151	149	149	154	148	149.8	2.32
0.1250	125	130	126	124	130	125	126.7	2.67
0.1875	108	110	108	108	108	107	108.2	.98
0.2500	94	96	97	98	97	97	96.5	1.38

OBLIQUE INCIDENCE

X							AVG.	STD DEV
0.0625	126	125	124	125	128	124	125.3	1.51
0.1250	102	102	100	102	104	101	101.8	1.34
0.1875	85	85	84	85	87	86	85.3	1.03
0.2500	74	75	75	75	76	75	75.0	.63

By Chauvenet's Criterion, data will be excluded where probability of occurrence would be less than $\frac{1}{2n}$. For six readings this is .0833. Assuming a Gaussian distribution of errors on the readings, this represents 1.73σ away from the mean before the datum becomes suspect. Table VII shows the upper and lower limits of acceptable data.

TABLE VII

LIMITS OF ACCEPTABLE DATA

	NORMAL INCIDENCE		OBLIQUE INCIDENCE	
X	UPPER BOUND	LOWER BOUND	UPPER BOUND	LOWER BOUND
0.0625	153.8	145.8	127.9	122.7
0.1250	131.3	122.0	104.1	99.5
0.1875	109.9	106.5	87.1	83.5
0.2500	98.9	94.1	76.1	73.9

Data falling outside of these ranges were eliminated and new averages computed. These results are listed in Table VIII.

TABLE VIII

SMOOTHED CIRCULAR HOLE COMPENSATOR DATA

DATA POINT	COMPENSATOR READINGS	
(in.)	Cn	$C_{\theta x}$
0.0625	149.0	124.8
0.125	126.7	101.8
0.1875	107.8	85.3
0.250	97.0	75.0

Extrapolating to the Edge of the Hole

Because it is difficult to measure the fringe count right at the edge of the hole, these data were plotted and extrapolated back to that point. It was found that log log values of the compensator readings plotted linearly

with x. The best fit was obtained by using the first three points.

$$\log (\log C_{\theta x}) = 0.3390 - 0.2853X \tag{130}$$

with R = -.9996. Using the value for x = 0,

$$C_{\theta x} = 152.31$$

For this Compensator, 47 counts constituted 1 fringe.

$$N_{\theta x} = 3.24$$

Similarly for the normal incidence fringes,

$$\log (\log C_N) = 0.3517 - 0.2323X \tag{131}$$

with R = .99996. Using the value for x = 0,

$$C_N = 176.81$$

and

$$N = 3.76$$

At the edge of the hole the radial stress, σ_r, is zero, which requires for the two dimensional plane stress geometry that

$$\varepsilon_r = -\bar{\nu}\,\varepsilon_\theta \tag{132}$$

Substituting equations (128) and (129) into equation (132), a relationship is found between $N_{\theta x}$ and N for all $\bar{\nu}$ at

the hole boundary.

$$N_{\theta x} = 0.8499\,N \tag{133}$$

After extrapolation the measured values of N = 3.76 and $N_{\theta x}$ = 3.24 check out to within 1.3% of the theoretical values from equation (133).

Accounting for Poisson's Ratio Mismatch

These fringe values are extrapolated from interior regions where $\bar{\nu}$ = .3256; however, at the edge of the hole, $\bar{\nu}$ = .3793; therefore, they must be adjusted to the appropriate Poisson's Ratio value. This is done by knowing that at the boundary the hoop stress is given by

$$\sigma_\theta = \frac{E_s F_\varepsilon N}{1+\bar{\nu}} \tag{134}$$

For a given σ_θ existing at the edge of the hole, the relation between the photoelastic readings for a different Poisson's Ratio is given from (134) to be

$$\frac{N_1}{1+\bar{\nu}_1} = \frac{N_2}{1+\bar{\nu}_2} \tag{135}$$

This, of course, assumes E_s and F_ε are held constant. Thus for our case, $\bar{\nu}_1$ = .3793 and $\bar{\nu}_2$ = .3256, and

$$N\Big]_{\bar{\nu}=.3793} = 1.0405\,N\Big]_{\bar{\nu}=.3256}$$

The actual normal incidence fringe value at the edge of the hole is now

$$N = (1.0405)(3.77) = 3.91$$

To find the corresponding value for the oblique incidence fringe, equation (133) is used in conjunction with equation (135).

$$N_{\theta x}\Big]_{\bar{\nu}=.3793} = 1.0405\, N_{\theta x}\Big]_{\bar{\nu}=.3256} \qquad (136)$$

From this the value of $N_{\theta x}$ at the edge of the hole is

$$N_{\theta x} = (1.0405)(3.24) = 3.37$$

The last correction to the data is for reinforcement, which for these materials is a factor of 1.0162 from equation (39).

$$N = 3.98 \qquad N_{\theta x} = 3.43$$

Check against Numerical Solution

A check can now be made against the numerical solution, which for this geometry and loading is given by a finite element solution developed by Kaiser (4) to be σ_θ = 51,678 psi. Using N = 3.98, the extrapolated photoelastic measurements

give from equation (134).

$$\sigma_\theta = \frac{(10.12\times10^6)(1764\times10^{-6})(3.98)}{1.3793} = 51,511 \text{ psi}$$

This value is within 0.3% of the finite element value. This is surprisingly good agreement.

Check of Stress Distribution

A check of the accuracy of the photoelastic work was also made on the stress distribution away from the hole by means of a finite element solution. The criteria established to determine uniform boundary stress distribution was uniformity in nodal displacements along the loaded edge as discussed by Segerlind (9). In the models used for FINITE ELEMENT ANALYSIS (FEA) in this report, nodal displacements were uniform to within 0.1%, and the resulting stress distribution was uniform axially to within 0.1% at the panel ends. In all cases two-dimensional, eight noded, isoparametric elements were used. These higher order elements cannot be loaded in an "intuitive" manner, as discussed by Zienkiewicz (10). Fig. 13 shows the nodal loading required to obtain a uniform surface load.

Element Meshes

Two meshes were developed for each panel analyzed. A reasonable effort was made to keep element corner angles as close to 90° as possible to reduce the effect of element

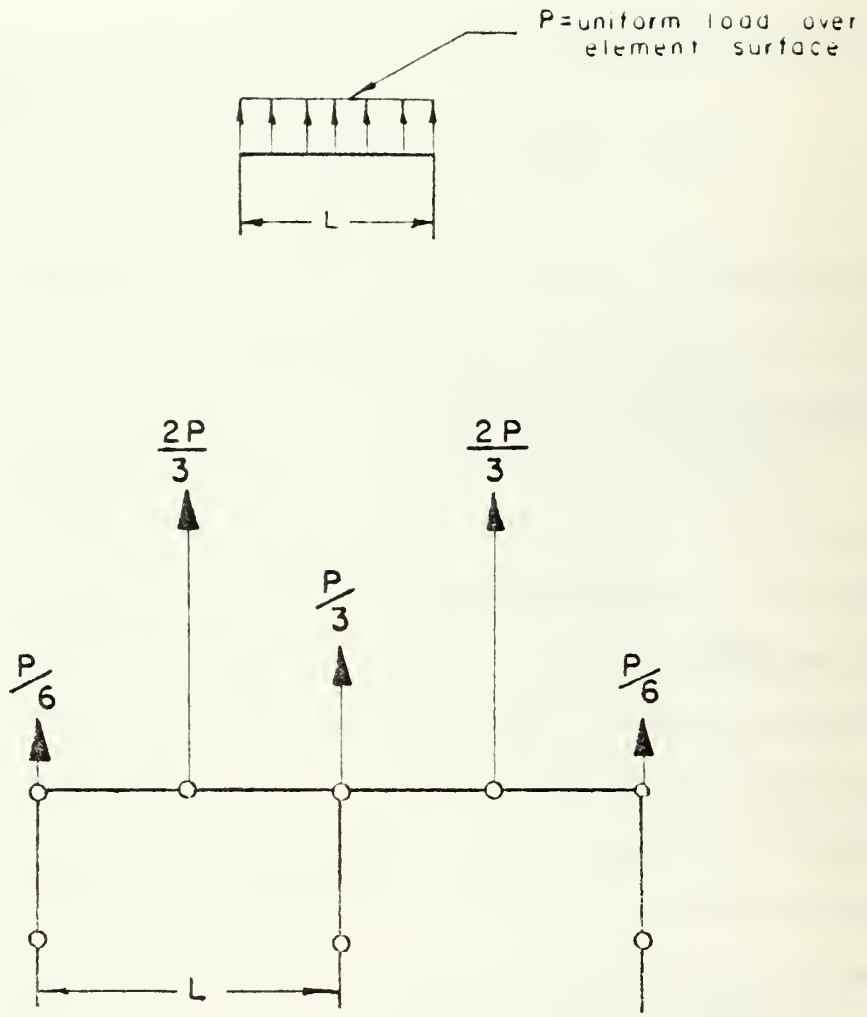

FIGURE 13

NODAL LOADING DIAGRAM

distortion discussed by Hopkins and Gifford (11). All meshes modeled a quarter of the actual panel by using the two axes of symmetry as is common practice in FEA. The step from course to fine element meshes was made so that each element in the course mesh was subdivided into four smaller elements of the same type. Such a mesh subdivision can be expected to give monotonic convergence of results, as shown by Cook (12), and allow extrapolation to results of an infinitely fine mesh. Figures 14 and 15 illustrate the element meshes used in this analysis.

Using ADINA

Once the mesh was developed, input data was prepared in accordance with the ADINA user's manual (13). This same set of data was used as input for PSAP1, the plot routine, to check for errors and provide a graphical display of the element mesh. After preprocessing by PSAP1, the data is entered into ADINA for analysis. In the case of linear analysis, two types of stress output may be specified, nodal point or Gauss integration point. Nodal point output can be computed for up to eight node point stresses for each element. Since 2x2 Gauss integration was used, four Gauss point stresses were computed for each element. The 2x2 Gauss integration is recognized as the most efficient integration order for this type of analysis [Ref. 10, p. 284]. The linear analysis used an isotropic linear elastic material

28 ELEMENTS (ISOPARAMETRIC)

111 NODES

192 DEGREES OF FREEDOM

DIMENSIONS

λ	W	L	RADIUS
0.2	5"	25"	1"
0.25	4.0625"	20"	1"

$$\lambda = \frac{\text{RADIUS}}{W}$$

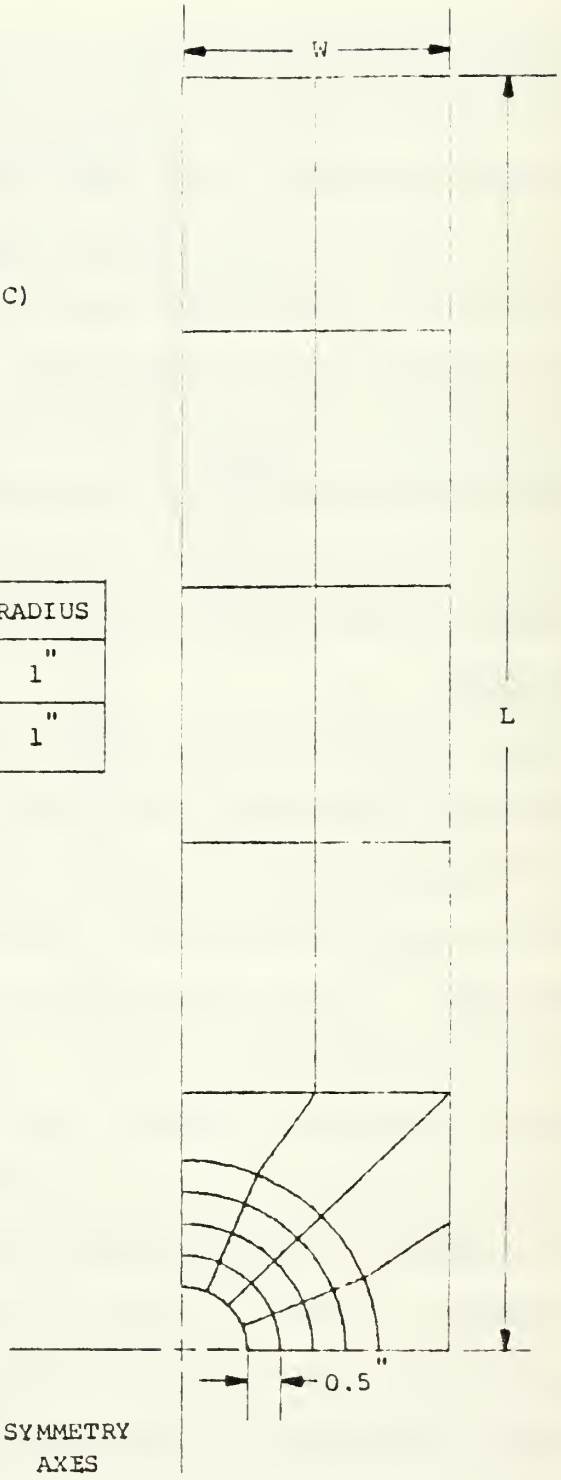

FIGURE 14

COURSE MESH FOR CIRCULAR HOLES

A SUBDIVISION OF COURSE MESH

112 ELEMENTS (ISOPARAMETRIC)

389 NODES

720 DEGREES OF FREEDOM

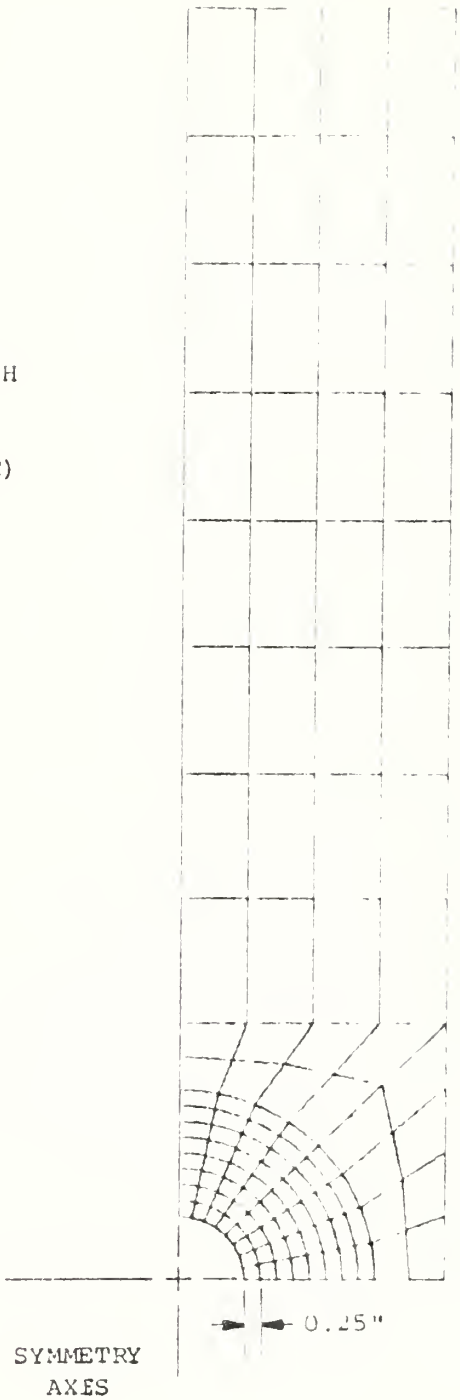

FIGURE 15

FINE MESH FOR CIRCULAR HOLES

model (MODEL "1" in Ref. 4) which required input of tensile modulus and material properties.

For static analyses ADINA uses a time function method to apply loads in steps. Linear analysis loading was accomplished in a single step to a nominal value of 3,000 lbs load. The stress output from ADINA is a listing of nodal or Gauss point stresses for each element. Since the only area of interest in this analysis was the distribution of stresses along the reduced cross-section, no large post-processing program was developed or used. All final computations using ADINA output data were accomplished on a HEWLETT-PACKARD 9830A calculator, using short programs coded in BASIC. If more extensive stress distribution information were desired, some form of automated post-processing would be necessary to reduce the computational workload. At a minimum, nodal stress outputs by ADINA must be averaged to obtain unique values of stress at nodes shared by more than one element.

Richardson Extrapolation

The use of course and fine meshes allows extrapolation to an infinitely fine mesh by means of the Richardson extrapolation (14) where:

$$\sigma_{extrap} = \frac{\sigma_c (h_F)^m - \sigma_F (h_c)^m}{h_F^m - h_c^m} \qquad (137)$$

where

σ_{extrap} = extrapolated solution

σ_c = solution obtained with $h=h_c$

σ_F = solution obtained with $h=h_F$

h_c = linear dimension of course element

h_F = linear dimension of fine element

m = 2 (for this analysis)

The exponent m is determined by the order of the discretization error $O(h^m)$. Since h represents the length of an element, the element area is represented by h^2. In a two dimensional problem such as this, $O(h^m)$ is of the order of h^2, the area of an element. In the mesh refinement scheme used Equation (137) can be rewritten

$$\sigma_{extrap} = \frac{\sigma_c \left(\frac{h_F}{h_c}\right)^2 - \sigma_F \left(\frac{h_c}{h_c}\right)^2}{\left(\frac{h_F}{h_c}\right)^2 - \left(\frac{h_c}{h_c}\right)^2} \qquad (138)$$

thus

$$\sigma_{extrap} = \frac{\sigma_F - \frac{1}{4}\sigma_c}{\frac{3}{4}} \qquad (139)$$

Equation (139) then becomes the relation to obtain extrapolated stresses from coarse and fine mesh results in a two dimen-

sional analysis. Better extrapolations can be obtained by using three or more defined meshes, but the computational effort increases significantly.

Optimal Stress Locations and Local Smoothing

It is generally accepted that the most accurate sampling points for stresses are the Gauss integration points within the element [Ref. 10, p. 281]. In this analysis, the nodal points are of the greatest interest; thus a technique of local smoothing must be applied to the integration point stresses to obtain nodal stresses as reported by Hinton and Campbell (15). The nodal values obtained must then be averaged if shared by two or more elements.

Circular Holes in Linear Material

The FEA results for a circular hole in a finite width strip were used to validate the photoelastic procedures discussed earlier. The results of Howland (8) were compared to both the Gauss point smoothed results and the nodal output results in Fig. 16. The stress concentration factor, σ/σ_∞, is referenced to the far-field stress. The smoothed results give the best match to the results of Howland at the edge of the hole, and the only significant variation between the two FEA methods occurs within the first 0.25 inches from the edge. In order to obtain the 0.25 inch stress value for the coarse mesh, in the Gauss point smoothed result, a midside node value had to be obtained by the averaging method.

FIGURE 16

CIRCULAR HOLE λ=0.2 LINEAR RESULTS

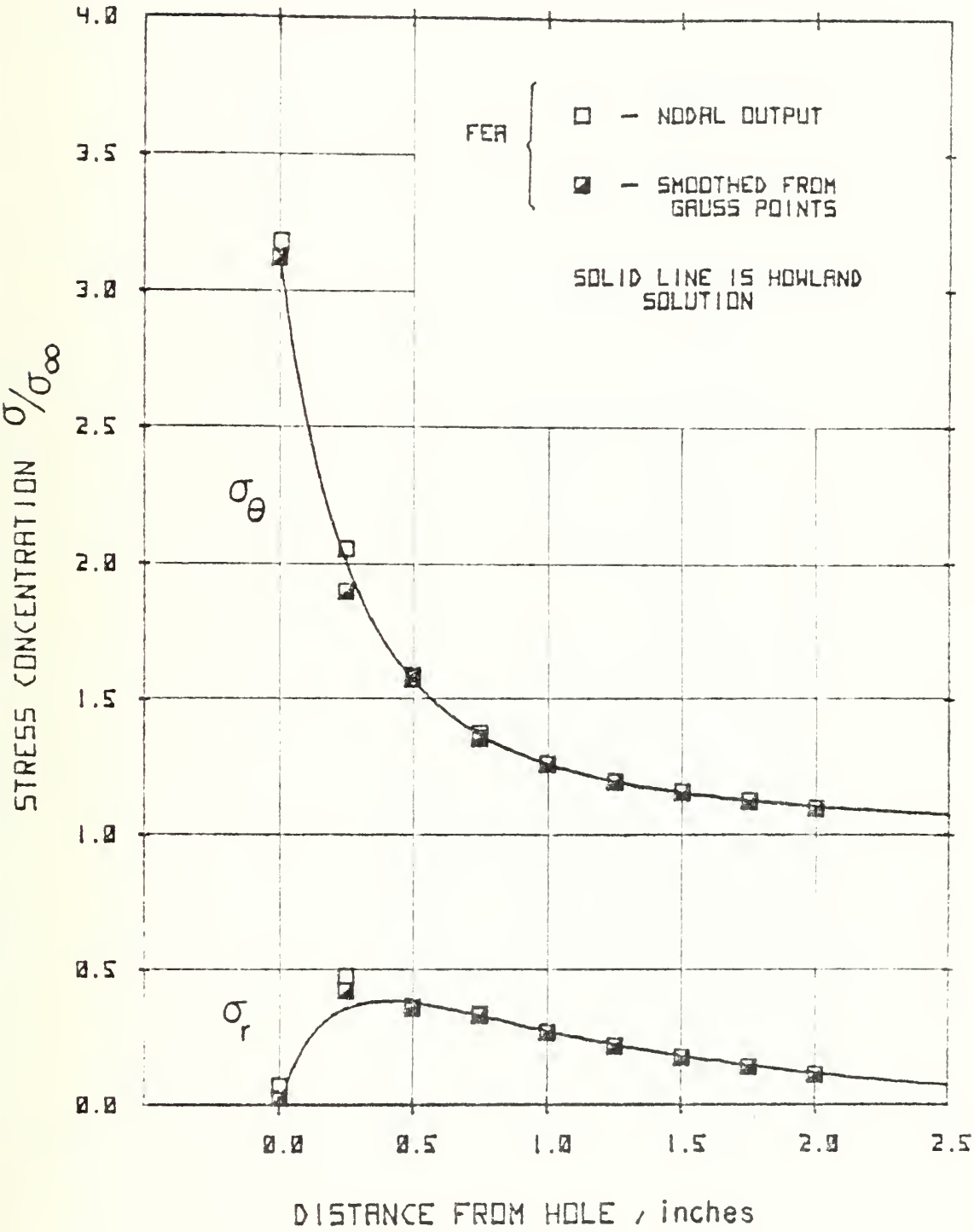

TABLE IX. $\lambda = 0.25$ FEA RESULTS - NODAL OUTPUT

DISTANCE FROM HOLE, in.	$\sigma_\infty = 4500$ psi σ_θ ,psi	σ_r ,psi
0.00	14745.5	329.8
0.25	9447.0	2181.1
0.50	7232.6	1599.3
0.75	6304.7	1473.5
1.00	5771.7	1139.6
1.25	5471.2	891.6
1.50	5266.9	671.0
1.75	5091.7	489.1
2.00	4940.2	354.5

TABLE X. $\lambda = 0.25$ FEA RESULTS - GAUSS OUTPUT

DISTANCE FROM HOLE, in.	$\sigma_\infty = 4500$ psi σ_θ ,psi	σ_r ,psi
0.00	14422.8	121.2
0.25	8721.2	1927.1
0.50	7317.1	1639.7
0.75	6218.6	1452.4
1.00	5779.6	1151.5
1.25	5453.3	891.0
1.50	5267.1	677.3
1.75	5085.9	486.9
2.00	4937.9	343.8

The linear distribution of smoothed stresses along the sides of the element, (15), appears to produce a less accurate result in this area of extreme stress gradient, when compared to ADINA's nodal output result. This tendency was noted in all cases; however, the peak stress values from smoothed results consistently gave better correlation with other investigators (16).

A circular hole with λ=0.25 was also analyzed and compared to the photoelastic experimental results. The stress distribution is given in Table IX and Table X. The data for the first two locations has been normalized and entered into Table XI to show a comparison with photoelastic results similarly normalized.

TABLE XI

COMPARISON OF STRESS DISTRIBUTION

	Finite Element		Photoelastic	
x	σ_r/σ_∞	σ_x/σ_∞	σ_r/σ_∞	$\sigma_\theta/\sigma_\infty$
0.00	-.0269	3.2051	-.1167	3.0780
0.25	.4282	2.0993	.4111	2.1627

Comparisons of the photoelastic data with the finite element show agreement within 3% and 4% on the average. This is not as good as the correlation made at the edge of the

hole where we required $\sigma_r = 0$. If σ_r is allowed to be whatever the readings show; then the correlation is in the 3% or 4% range; however as can be seen at x = 0, the finite element is not exact either, especially at these small x values.

Sensitivity Studies

At the edge of the hole where $\bar{\nu} = .3793$, the expressions for strain from equations (128) and (129) become

$$\varepsilon_r = 1.5798 \times 10^{-3} N - 2.4296 \times 10^{-3} N_{\theta x} \tag{140}$$

$$\varepsilon_\theta = 3.3438 \times 10^{-3} N - 2.4296 \times 10^{-3} N_{\theta x} \tag{141}$$

Substituting these expressions into the plane stress constitutive equations

$$\sigma_r = 2.0897 \times 10^4 N - 2.4587 \times 10^4 N_{\theta x} \tag{142}$$

$$\sigma_\theta = 2.8930 \times 10^4 N - 2.4587 \times 10^4 N_{\theta x} \tag{143}$$

The sensitivity of the stress is given by

$$d\sigma = \frac{\partial \sigma}{\partial N} dN + \frac{\partial \sigma}{\partial N_{\theta x}} dN_{\theta x} \tag{144}$$

Applying this to equations (142) and (143)

$$d\sigma_r = 2.0897 \times 10^4 dN - 2.4587 \times 10^4 d N_{\theta x} \quad (145)$$

$$d\sigma_\theta = 2.8930 \times 10^4 dN - 2.4587 \times 10^4 dN_{\theta x} \quad (146)$$

Selecting the maximum deviation of N and $N_{\theta x}$ as 1.73σ, where σ is the standard deviation of the smoothed data

$$dN = (1.73)(\pm 1.22) = \pm 2.11$$

$$dN_{\theta x} = (1.73)(\pm .84) = \pm 1.45$$

Then $d\sigma$ can have two values depending upon how the plus and minus signs couple up. The worst of these are:

$$d\sigma_r = \pm 1697 \text{ psi}$$

$$d\sigma_\theta = \pm 2057 \text{ psi}$$

These figures represent the maximum errors that would be expected due to misreading the fringe pattern, and they are approximately 4% on σ_θ and explains how non-zero results for σ_r arise.

CONCLUSIONS AND RESULTS

From very careful experimental procedures where no handbook values for material properties were used but all were carefully determined, photoelastic measurements checked theoretical results within 4%. This error included all errors in material properties, in operator readings and in equipment calibration. Without very careful and detailed measurements on every parameter, photoelastic results could easily be in error by 15% to 20%.

With this level of accuracy established by controlled laboratory procedures and calibrations of equipment in place, we will now proceed to study the elastic and plastic behavior of notches where fatigue failure originate.

REFERENCES

1. Frank E. Stenstrom, "Photoelastic Study of Elastic and Plastic Stress Fields in the Vicinity of a Notch", Master's Thesis, Naval Postgraduate School, Monterey, California, December 1980.

2. Amineo-Tuckerman Optical Strain Gage System Instructions No. 750, p.16, American Instrument Company, Inc. 1958.

3. ASTM 1980 Annual Book of Standards, Part 10, Standard E8-77a.

4. Michael J. Kaiser, "An Elastic-Plastic Finite Element Analysis of Notched Aluminum Panels", Master's Thesis, Naval Postgraduate School, Monterey, California, March 1981.

5. Micro-Measurement, Transverse Sensitivity Errors TN-137, undated, Vishay Intertechnology, Inc.

6. Walter Ramberg and William R. Osgood, "Description of Stress-Strain Curves by Three Parameters", NACA TN 902, July 1943.

7. J. W. Dally and I. Alfirevich, "Application of Birefringent Coatings to Glass-fiber-reinforced Plastics", Experimental Mechanics, Vol. 9, p. 97-102, 1969.

8. Howland, R.C.J., "Stress in a Strip of Finite Width, Which is Weakened by a Circular Hole," Philosophical Transactions of the Royal Society, Series A, V. 229, pp. 49-86, London, 1930.

9. Segerlind, L.J., Applied Finite Element Analysis, p. 251, Wiley, 1976.

10. Zienkiewicz, O.C., The Finite Element Method, 3d Ed., McGraw-Hill Ltd, 1977.

11. David W. Taylor Naval Ship Research and Development Center Report, Accuracy Loss in Distorted Isoparametric Finite Elements, by D. A. Hopkins and L. N. Gifford, September 1978.

12. Cook, R.D., Concepts and Applications of Finite Element Analysis, pp. 87-92, Wiley, 1974.

13. Massachusetts Institute of Technology Report 82448-1, A Finite Element Program for Automatic Dynamic Incremental Nonlinear Analysis (ADINA), by K. Bathe, September 1975 (revised May 1976).

14. Crandall, S.H., Engineering Analysis - A Survey of Numerical Procedures, pp. 171-173, McGraw-Hill, 1956.

15. Hinton, E., and Campbell, J.S., "Local and Global Smoothing of Discontinuous Finite Element Functions Using a Least Squares Method," International Journal for Numerical Methods in Engineering, V. 8, pp. 461-480, 1974.

16. Peterson, R.E., Stress Concentration Factors, pp. 20-36 and 111-150, Wiley, 1974.

APPENDIX A

Equations of Photoelasticity Coatings

$$\varepsilon_1 - \varepsilon_2 = \frac{f_\varepsilon N}{2h_c} = F_\varepsilon N \qquad \text{(A-1)}$$

$$\sigma_1^c - \sigma_2^c = \frac{f_\sigma N}{2h_c} = F_\sigma N \qquad \text{(A-2)}$$

$$f_\sigma = \left(\frac{E_c}{1+\nu_c}\right) f_\varepsilon \qquad \text{(A-3)}$$

$$f_\varepsilon = \frac{\lambda}{K} \qquad \text{(A-4)}$$

$$F_\sigma = \left(\frac{E_c}{1+\nu_c}\right) F_\varepsilon \qquad \text{(A-5)}$$

DISTRIBUTION LIST

		No. of Copies
1.	Defense Technical Information Center Attn: DDC-TCA Cameron Station, Bldg. 5 Alexandria, VA 22314	2
2.	Library, Code 0212 Naval Postgraduate School Monterey, CA 93940	2
3.	Dean of Research Code 012 Naval Postgraduate School Monterey, CA 93940	1
4.	Chairman Department of Aeronautics Code 67 Naval Postgraduate School Monterey, CA 93940	1
5.	Professor G. H. Lindsey Code 67Li Department of Aeronautics Naval Postgraduate School Monterey, CA 93940	3
6.	Dr. Dan Mulville Code 320B Naval Air Systems Command Washington, DC 20361	3